Radiative transitions and magnetic moments of the charmed and bottom vector mesons in chiral perturbation theory

Bo Wang,[1,2,*] Bin Yang,[1,†] Lu Meng,[1,‡] and Shi-Lin Zhu[1,2,3,§]

[1]*School of Physics and State Key Laboratory of Nuclear Physics and Technology, Peking University, Beijing 100871, China*

[2]*Center of High Energy Physics, Peking University, Beijing 100871, China*

[3]*Collaborative Innovation Center of Quantum Matter, Beijing 100871, China*

(Received 21 May 2019; published 29 July 2019)

In this work, we systematically study the radiative decays and magnetic moments of the charmed and bottom vector mesons with chiral perturbation theory up to one-loop level. We present the results in the SU(2) and SU(3) cases with the mass splitting in loop diagrams kept and unkept, respectively. The obtained decay rates for D^* and B^* mesons in the SU(3) case with the mass splitting kept are $\Gamma_{\bar{D}^{*0}\to\bar{D}^0\gamma}=16.2^{+6.5}_{-6.0}$ keV, $\Gamma_{D^{*-}\to D^-\gamma}=0.73^{+0.7}_{-0.3}$ keV, $\Gamma_{D_s^{*-}\to D_s^-\gamma}=0.32^{+0.3}_{-0.3}$ keV, and $\Gamma_{B^{*+}\to B^+\gamma}=0.58^{+0.2}_{-0.2}$ keV, $\Gamma_{B^{*0}\to B^0\gamma}=0.23^{+0.06}_{-0.06}$ keV, $\Gamma_{B_s^{*0}\to B_s^0\gamma}=0.04^{+0.03}_{-0.03}$ keV. The decay width for $D^{*-}\to D^-\gamma$ is consistent with the experimental measurement. As a byproduct, the full widths of $\bar{D}^{*0}$ and D_s^{*-} are $\Gamma_{\rm tot}(\bar{D}^{*0})\simeq 77.7^{+26.7}_{-20.5}$ keV and $\Gamma_{\rm tot}(D_s^{*-})\simeq 0.62^{+0.45}_{-0.50}$ keV, respectively. We also calculate the magnetic moments of the heavy vector mesons. The analytical chiral expressions derived in our work shall be helpful for the extrapolations of lattice QCD simulations in the future.

DOI: 10.1103/PhysRevD.100.016019

I. INTRODUCTION

Electromagnetic form factors play a very important role in mapping out the internal structures of nucleons, offering valuable information about the distribution of the constituent quarks and the gluon degree of freedom in nucleons [1–4]. Probing the shape and inner structure of hadrons still remains an intriguing and challenging topic. Especially in recent decades, a large number of exotic states have been observed in experiments, many of which cannot be readily reconciled with the predictions of the conventional quark models [5–7].

Magnetic moments can be related to the form factors by extrapolating the form factor $\mathcal{G}_M(q^2)$ to zero moment transfer [8]. Unlike protons and neutrons, the vast majority of hadronic states are unstable against strong interactions [9]. Thus, their magnetic moments cannot be directly measured in the conventional ways due to their very short lifetime. Therefore, the radiative transition becomes a very effective way to help us catch a glimpse of quark dynamics in the hadrons. In addition, the quark model cannot give the nonanalytic dependence of the magnetic moments, such as the $\log X$ term. These terms are much more difficult to naively estimate and may sometimes be singular in order to give the much enhanced contributions which cannot be predicted accurately unless carefully calculated.

In this work, we focus on the charmed and bottom vector mesons, i.e., ($\bar{D}^{*0}$, D^{*-}, D_s^{*-}) and (B^{*+}, B^{*0}, B_s^{*0}). As a consequence of heavy quark spin symmetry, the mass shifts between these spin triplets and singlets are generally small. Because of the small phase space, the dominant decay channels are one-pion emission transitions and radiative decays for the charmed vector mesons, while only radiative decays are allowed for the bottom vector mesons.

From Ref. [9], only the width of $D^{*\pm}\to D^\pm\gamma$ is known by combining the decay branching ratio and the total width of $D^{*\pm}$. For the other radiative decay modes, only the branching ratios are available, and the absolute widths are still absent in experiments. Even worse, there is no experimental information for the radiative transitions of the B^* mesons.

Many theoretical methods have been applied to study the radiative decays of the D^* and B^* mesons, such as various quark models [10–15], heavy quark effective theory and the vector meson dominance model [16], quark-potential models [17–22], QCD sum rules [23–25], lattice QCD simulations [26], the constituent quark-meson model [27],

*bo-wang@pku.edu.cn
†bin_yang@pku.edu.cn
‡lmeng@pku.edu.cn
§zhusl@pku.edu.cn

chiral effective field theory [28–31], the extended Nambu–Jona-Lasinio model [32,33], and so on.

Here, we adopt the SU(3) chiral perturbation theory (χPT) to investigate the radiative decay properties and magnetic moments of the D^* and B^* mesons. The framework of χPT has been widely used to study the radiative decays and magnetic moments of the charmed and bottom vector mesons[1] [28–31], the octet baryons [34,35], the doubly charmed and bottom heavy baryons [36–39], and the singly heavy baryons [40–43], as well as the related chiral quark-soliton model for singly heavy baryons [44,45]. In our calculations, we construct the effective Lagrangians with chiral symmetry and heavy quark symmetry up to $\mathcal{O}(p^4)$. There are two independent low-energy constants (LECs) at the leading order, which correspond to the contributions from the light quark and heavy quark electromagnetic currents, respectively. These two LECs can be estimated with the quark model or other theoretical methods. The contributions from the tree diagrams at next-to-leading order can be absorbed into the ones from leading order. At next-to-next-to-leading order, the tree diagram incorporates three independent LECs, which cannot be determined due to lack of experimental data. We present our numerical results up to $\mathcal{O}(p^4)$, and we consider the contributions from $\mathcal{O}(p^4)$ tree diagrams as errors.

Our numerical results are calculated in both the SU(2) and SU(3) cases with the mass splitting kept and unkept in loop diagrams. The partial decay widths of $D^{*-} \to D^-\gamma$ predicted in different scenarios are consistent with the experimental data.

This paper is organized as follows: The definitions of the electromagnetic form factors and magnetic moments are given in Sec. II. The effective Lagrangians are constructed in Sec. III. The analytical expressions and numerical results for the transition magnetic moments and magnetic moments are presented in Secs. IV and V, respectively. A summary is given in Sec. VI. Some supplemental materials for the B^* mesons, the loop integrals, and an estimation of the light quark mass with the vector meson dominance model are collected in the Appendixes A, B, and C, respectively.

II. ELECTROMAGNETIC FORM FACTORS AND MAGNETIC MOMENTS

We first consider the radiative transition process $V \to P\gamma$, where V stands for the vector mesons (D^* or B^*), and P denotes the pseudoscalar mesons (D or B). The M1 transition form factor $\mu'(q^2)$ can be defined through a covariant expression of the hadronic matrix elements [31],

$$\langle P(p')|J^{\mu}_{em}(q^2)|V(p,\varepsilon_V)\rangle = e\mu'(q^2)\epsilon^{\mu\nu\alpha\beta}p_\nu q_\alpha \varepsilon_{V\beta}, \quad (1)$$

where J^{μ}_{em} is the electromagnetic current at the hadronic level, $q_\alpha = (p-p')_\alpha$ is the transferred momentum, and $\varepsilon_{V\beta}$ denotes the polarization vector of the initial vector meson.

The interaction Hamiltonian can then be written as

$$H_{\rm int} = \int d^3x e A_\mu J^{\mu}_{em}, \quad (2)$$

where A_μ is the photon field.

For a heavy meson M that is composed of a heavy antiquark $\bar{Q}$ and a light quark q, the ground spin doublet (P, P^*) can be represented by a 4×4 Dirac-type matrix $\mathcal{H}$. We use $\mathcal{H}(p)$ and $\mathcal{H}(v)$ to denote the heavy meson fields in relativistic and heavy meson effective theory (HMET) convention, respectively. They can be related with each other by

$$|\mathcal{H}(p)\rangle = \sqrt{m_H}[|\mathcal{H}(v)\rangle + \mathcal{O}(1/m_H)]. \quad (3)$$

Then, in the framework of HMET, Eq. (1) can be reexpressed as

$$\langle P(p')|J^{\mu}_{em}|V(p,\varepsilon_V)\rangle = e\sqrt{m_V m_P}\mu'(q^2)\epsilon^{\mu\nu\alpha\beta}v_\nu q_\alpha \varepsilon_{V\beta}, \quad (4)$$

where the recoil effect is negligible in the above equation.

With the above preparation, one can easily get the expression of the decay rate,

$$\Gamma[V\to P\gamma] = \frac{1}{3}\int d\Omega_{\hat{q}}\frac{1}{32\pi^2}\frac{|\boldsymbol{q}|}{m_V^2}\sum|\mathcal{M}|^2, \quad (5)$$

where $\mathcal{M}$ represents the transition amplitude, and a sum over the final-state photon polarization and an average over the initial V polarization have been performed.

Explicitly, we have

$$\Gamma[V\to P\gamma] = \frac{\alpha}{3}\frac{m_P}{m_V}|\mu'(0)|^2|\boldsymbol{q}|^3, \quad (6)$$

where $\alpha = 1/137$ is the fine-structure constant. The transition magnetic moment $\mu_{V\to P\gamma}$ can be defined as

$$\mu_{V\to P\gamma} = \frac{e}{2}\mu'(0). \quad (7)$$

In the following, we derive the magnetic moment of a vector meson. The matrix elements of $J^{\mu}_{em}(q^2)$ are defined in terms of the standard Lorentz covariant decomposition [46]:

[1]In Refs. [28,29], Cho *et al.* and Cheng *et al.* calculated the decay widths of $D^* \to D\gamma$ and $B^* \to B\gamma$, respectively, at the tree level in the heavy hadron chiral theory. Our Lagrangians are the same as those in Refs. [28,29] at leading order. In Ref. [30], Amundson *et al.* investigated the same process with the same framework to next-to-leading order. But the heavy quark spin symmetry breaking effect is ignored.

$$\begin{aligned}\mathcal{G}^{\mu}(q^2) &= \langle V(p',\varepsilon'^*)|J^{\mu}_{em}(q^2)|V(p,\varepsilon)\rangle \\ &= -\mathcal{G}_1(q^2)(\varepsilon\cdot\varepsilon'^*)(p+p')^{\mu} \\ &\quad + \mathcal{G}_2(q^2)[(\varepsilon\cdot q)\varepsilon'^{*\mu} - (\varepsilon'^*\cdot q)\varepsilon^{\mu}] \\ &\quad + \mathcal{G}_3(q^2)\frac{(\varepsilon\cdot q)(\varepsilon'^*\cdot q)}{2m_V^2}(p+p')^{\mu}. \end{aligned} \tag{8}$$

This expression can be simplified under the Breit frame. In our calculations, we define

$$q^{\mu} = (p-p')^{\mu} = (0,\boldsymbol{Q}), \quad \boldsymbol{Q} = Q\hat{z}, \quad p^{\mu} = \left(p^0, \frac{1}{2}\boldsymbol{Q}\right),$$
$$p'^{\mu} = \left(p^0, -\frac{1}{2}\boldsymbol{Q}\right), \quad -q^2 = Q^2 \geq 0, \quad p^0 = \sqrt{m_V^2 + \frac{1}{4}Q^2}.$$

A straightforward derivation under the Breit frame gives the time component of $\mathcal{G}^{\mu}(q^2)$ as

$$\begin{aligned}\mathcal{G}^0(Q^2) = 2p^0\Bigg\{&\mathcal{G}_C(Q^2)(\boldsymbol{\varepsilon}\cdot\boldsymbol{\varepsilon}'^*) \\ &+ \frac{\mathcal{G}_Q(Q^2)}{2m_V^2}\left[(\boldsymbol{\varepsilon}\cdot\boldsymbol{Q})(\boldsymbol{\varepsilon}'^*\cdot\boldsymbol{Q}) - \frac{1}{3}(\boldsymbol{\varepsilon}\cdot\boldsymbol{\varepsilon}'^*)Q^2\right]\Bigg\}, \end{aligned} \tag{9}$$

where $\mathcal{G}_C$ and $\mathcal{G}_Q$ represent charge and quadrupole form factors, respectively. In deriving Eq. (9), we have used the transverse condition of the initial- and final-state polarization vectors; i.e., $p\cdot\varepsilon = 0$ and $p'\cdot\varepsilon'^* = 0$.

Similarly, the space component of $\mathcal{G}^{\mu}(q^2)$ is

$$\begin{aligned}\boldsymbol{\mathcal{G}}(Q^2) &= \mathcal{G}_2(Q^2)[(\boldsymbol{\varepsilon}'^*\cdot\boldsymbol{Q})\boldsymbol{\varepsilon} - (\boldsymbol{\varepsilon}\cdot\boldsymbol{Q})\boldsymbol{\varepsilon}'^*] \\ &= 2p^0\frac{\mathcal{G}_M(Q^2)}{2m_V}[(\boldsymbol{\varepsilon}'^*\cdot\boldsymbol{Q})\boldsymbol{\varepsilon} - (\boldsymbol{\varepsilon}\cdot\boldsymbol{Q})\boldsymbol{\varepsilon}'^*], \end{aligned} \tag{10}$$

where $\mathcal{G}_M$ is the magnetic dipole form factor. The expressions of $\mathcal{G}_C$, $\mathcal{G}_Q$, and $\mathcal{G}_M$ read

$$\begin{aligned}\mathcal{G}_C &= \mathcal{G}_1 + \frac{2}{3}\eta\mathcal{G}_Q, \\ \mathcal{G}_Q &= \mathcal{G}_3 + \mathcal{G}_2(1+\eta)^{-1} + \frac{1}{2}\mathcal{G}_1(1+\eta)^{-1}, \\ \mathcal{G}_M &= \mathcal{G}_2, \end{aligned} \tag{11}$$

where $\eta = Q^2/(4m_V^2)$.

III. EFFECTIVE LAGRANGIANS

A. The leading-order chiral Lagrangians

We first introduce the Lagrangian of Goldstone bosons and photon. The octet of the light pseudoscalar field is represented by the field $U(x) = e^{i\phi/f_\phi}$ with

$$\phi = \begin{pmatrix} \pi^0 + \frac{1}{\sqrt{3}}\eta & \sqrt{2}\pi^+ & \sqrt{2}K^+ \\ \sqrt{2}\pi^- & -\pi^0 + \frac{1}{\sqrt{3}}\eta & \sqrt{2}K^0 \\ \sqrt{2}K^- & \sqrt{2}\bar{K}^0 & -\frac{2}{\sqrt{3}}\eta \end{pmatrix}, \tag{12}$$

where the η field denotes the octet η_8. In the SU(3) quark model, the η meson is regarded as the mixing of the octet η_8 and the singlet η_0 with $|\eta\rangle = \cos\theta|\eta_8\rangle - \sin\theta|\eta_0\rangle$ [47], where $\theta \simeq -19.1°$ is determined by the experimental measurements [48,49]. Because the mixing angle is not very large and the η field only serves as the quantum fluctuations in the loops, the mixing effect is ignored in our calculations.

The definitions of the chiral connection and axial-vector current are

$$\Gamma_{\mu} \equiv \frac{1}{2}[u^{\dagger}(\partial_{\mu} - ir_{\mu})u + u(\partial_{\mu} - il_{\mu})u^{\dagger}], \tag{13}$$

$$u_{\mu} \equiv \frac{i}{2}[u^{\dagger}(\partial_{\mu} - ir_{\mu})u - u(\partial_{\mu} - il_{\mu})u^{\dagger}], \tag{14}$$

where

$$u^2 = U = \exp\left(\frac{i\phi}{f_\phi}\right), \qquad r_{\mu} = l_{\mu} = -eQA_{\mu}, \tag{15}$$

and $Q = Q_l = \mathrm{diag}(2/3, -1/3, -1/3)$ represents the electric charge matrix of the light current J^{ℓ}_{μ},

$$J^{\ell}_{\mu} = \frac{2}{3}\bar{u}\gamma_{\mu}u - \frac{1}{3}\bar{d}\gamma_{\mu}d - \frac{1}{3}\bar{s}\gamma_{\mu}s. \tag{16}$$

Here, f_ϕ is the decay constant of the light pseudoscalar mesons. The experimental values of f_ϕ for $\phi = \pi$, K, and η are $f_\pi = 92.4$ MeV, $f_K = 113$ MeV, and $f_\eta = 116$ MeV, respectively.

The leading-order $[\mathcal{O}(p^2)]$ Lagrangian for the interaction of the light pseudoscalars and photon reads [36–38]

$$\mathcal{L}^{(2)}_{\phi\gamma} = \frac{f_\phi^2}{4}\mathrm{Tr}[\nabla_{\mu}U(\nabla^{\mu}U)^{\dagger}], \tag{17}$$

where

$$\nabla_{\mu}U = \partial_{\mu}U - ir_{\mu}U + iUl_{\mu}. \tag{18}$$

We use $\mathrm{Tr}(X)$ and $\langle X\rangle$ to denote the traces for X in flavor space and spinor space, respectively.

We construct the effective Lagrangian for the heavy mesons with the superfield $\mathcal{H}$. For a heavy meson composed of a heavy antiquark $\bar{Q}$ and a light quark q, the superfield $\mathcal{H}$ is defined as

$$\mathcal{H} = (P^*_\mu \gamma^\mu + iP\gamma_5)\frac{1-\not{v}}{2},$$
$$\bar{\mathcal{H}} = \gamma^0 \mathcal{H}^\dagger \gamma^0 = \frac{1-\not{v}}{2}(P^{*\dagger}_\mu \gamma^\mu + iP^\dagger \gamma_5), \quad (19)$$

where for the charmed mesons

$$P = (\bar{D}^0, D^-, D_s^-), \qquad P^* = (\bar{D}^{0*}, D^{*-}, D_s^{*-}), \quad (20)$$

and for the bottom mesons

$$P = (B^+, B^0, B_s^0), \qquad P^* = (B^{*+}, B^{*0}, B_s^{*0}). \quad (21)$$

The leading-order Lagrangians for describing the interactions between the heavy matter field and light pseudoscalars are [50,51]

$$\mathcal{L}^{(1)}_{H\phi} = -i\langle \bar{\mathcal{H}} v\cdot \mathcal{D}\mathcal{H}\rangle - \frac{1}{8}\Delta\langle \bar{\mathcal{H}}\sigma^{\mu\nu}\mathcal{H}\sigma_{\mu\nu}\rangle + g\langle \bar{\mathcal{H}}\not{u}\gamma_5\mathcal{H}\rangle, \quad (22)$$

where the covariant derivative $\mathcal{D}_\mu = \partial_\mu + \Gamma_\mu$. Here, the electric charge matrix in Γ_μ should be replaced by those corresponding to the heavy mesons. For instance, $Q = Q_D = \mathrm{diag}(0,-1,-1)$ for $(\bar{D}^{*0}, D^{*-}, D_s^{*-})$, and $Q = Q_B = \mathrm{diag}(1,0,0)$ for $(B^{*+}, B^{*0}, B_s^{*0})$, respectively. The second term in Eq. (22) is due to the mass difference between P and P^*, and $\Delta = m_{P^*} - m_P$ stands for the mass splitting. g represents the axial coupling constant. For the D meson, its value can be extracted by the partial decay width of $D^{*+} \to D^0\pi^+$ [9,52], while for the B meson, g can only be determined via theoretical methods, such as the quark model [31] and lattice QCD [53,54].

We also need the Lagrangians to describe the (transition) magnetic moments at the tree level, which can be written as [36–38]

$$\mathcal{L}^{(2)}_{H\gamma} = \tilde{a}\langle \bar{\mathcal{H}}\sigma^{\mu\nu}\tilde{f}^+_{\mu\nu}\mathcal{H}\rangle + a\langle \mathcal{H}\sigma^{\mu\nu}\bar{\mathcal{H}}\rangle \mathrm{Tr}(f^+_{\mu\nu}), \quad (23)$$

where $\tilde{a}$ and a are two LECs. The first and second terms correspond to the contributions from the light quark and the heavy antiquark, respectively. The field strength tensors $\tilde{f}^+_{\mu\nu}$ and $f^+_{\mu\nu}$ are defined as

$$f^R_{\mu\nu} = f^L_{\mu\nu} = -eQ(\partial_\mu A_\nu - \partial_\nu A_\mu),$$
$$f^\pm_{\mu\nu} = u^\dagger f^R_{\mu\nu} u \pm u f^L_{\mu\nu} u^\dagger,$$
$$\tilde{f}^\pm_{\mu\nu} = f^\pm_{\mu\nu} - \frac{1}{3}\mathrm{Tr}(f^\pm_{\mu\nu}), \quad (24)$$

where $Q = Q_D$ for the D mesons and $Q = Q_B$ for the B mesons. From Eq. (24), we can see that $\tilde{f}^+_{\mu\nu}$ is proportional to Q_l and traceless. $f^+_{\mu\nu}$ is not traceless, because it contains the electric charge matrix of the heavy mesons. One can also understand Eq. (23) from the standpoint of group representation theory. Recall that $3 \otimes \bar{3} = 1 \oplus 8$, and the operator $\tilde{f}^+_{\mu\nu}$ transforms as the adjoint representation. Thus, the two terms in Eq. (23) correspond to $8 \otimes 8 \to 1$ and $1 \otimes 1 \to 1$, respectively.

In the following, we construct the Lagrangian for the interactions of the heavy mesons and light pseudoscalar mesons at $\mathcal{O}(p^2)$, which will contribute to the $\mathcal{O}(p^4)$ magnetic moment at the one-loop level [36–38]:

$$\mathcal{L}^{(2)}_{H\phi\phi} = ib\langle \bar{\mathcal{H}}\sigma^{\mu\nu}[u_\mu, u_\nu]\mathcal{H}\rangle. \quad (25)$$

Actually, the tensor structure sandwiched between $\bar{\mathcal{H}}$ and $\mathcal{H}$ in Eq. (25) can also be $\{u_\mu, u_\nu\}$ and $\mathrm{Tr}(u_\mu u_\nu)$. For the SU(3) group representations,

$$3 \otimes \bar{3} = 1 \oplus 8,$$
$$8 \otimes 8 = 1 \oplus 8_1 \oplus 8_2 \oplus 10 \oplus \overline{10} \oplus 27. \quad (26)$$

The axial-vector current u_μ (or u_ν) transforms as the adjoint representation; thus $\mathrm{Tr}(u_\mu u_\nu)$, $[u_\mu, u_\nu]$, and $\{u_\mu, u_\nu\}$ belong to the 1, 8_1, and 8_2 flavor representations, respectively. But $\mathrm{Tr}(u_\mu u_\nu)$ and $\{u_\mu, u_\nu\}$ would vanish when they are contracted with $\sigma^{\mu\nu}$, because of the symmetric Lorentz indices μ and ν. Therefore, only one independent term containing $[u_\mu, u_\nu]$ survives in Eq. (25).

B. The next-to-leading-order chiral Lagrangians

The electromagnetic chiral Lagrangians at $\mathcal{O}(p^3)$ read [43]

$$\mathcal{L}^{(3)}_{H\gamma} = -i\tilde{c}\langle \bar{\mathcal{H}}\sigma^{\mu\nu} v\cdot\nabla \tilde{f}^+_{\mu\nu}\mathcal{H}\rangle - ic\langle \mathcal{H}\sigma^{\mu\nu}\bar{\mathcal{H}}\rangle v\cdot\nabla \mathrm{Tr}(f^+_{\mu\nu}). \quad (27)$$

The structure is similar to those in Eq. (23). The possible contributions that include the covariant derivative $\mathcal{D}_\mu$ can be absorbed into the LECs $\tilde{c}$ and c with the equation of motion of the heavy mesons. Meanwhile, the contributions from Eq. (27) can be absorbed into Eq. (23) by renormalizing the LECs $\tilde{a}$ and a, i.e.,

$$\tilde{a} \rightarrowtail \tilde{a} + \tilde{c}\, v\cdot q, \qquad a \rightarrowtail a + c\, v\cdot q. \quad (28)$$

C. The next-to-next-to-leading-order chiral Lagrangians

At this order, we also employ group representation methods to construct the electromagnetic chiral Lagrangians (one can find the possible flavor structures in Table I). The detailed form reads [36–38]

$$\mathcal{L}^{(4)}_{H\gamma} = \tilde{d}\langle \mathcal{H}\sigma^{\mu\nu}\tilde{\chi}_+\bar{\mathcal{H}}\rangle \mathrm{Tr}(f^+_{\mu\nu}) + \bar{d}\langle \bar{\mathcal{H}}\sigma^{\mu\nu}\mathcal{H}\rangle \mathrm{Tr}(\tilde{f}^+_{\mu\nu}\tilde{\chi}_+)$$
$$+ d\langle \bar{\mathcal{H}}\sigma^{\mu\nu}\{\tilde{\chi}_+, \tilde{f}^+_{\mu\nu}\}\mathcal{H}\rangle, \quad (29)$$

TABLE I. The possible flavor structures of the $\mathcal{O}(p^4)$ Lagrangians that contribute to the magnetic moments.

Group representations	$1\otimes 1\to 1$	$1\otimes 8\to 8$	$8\otimes 1\to 8$	$8\otimes 8\to 1$	$8\otimes 8\to 8_1$	$8\otimes 8\to 8_2$
Flavor structures	$\mathrm{Tr}(\chi_+)\mathrm{Tr}(f_{\mu\nu}^+)$	$\mathrm{Tr}(\chi_+)\tilde{f}_{\mu\nu}^+$	$\tilde{\chi}_+\mathrm{Tr}(f_{\mu\nu}^+)$	$\mathrm{Tr}(\tilde{\chi}_+\tilde{f}_{\mu\nu}^+)$	$[\tilde{\chi}_+,\tilde{f}_{\mu\nu}^+]$	$\{\tilde{\chi}_+,\tilde{f}_{\mu\nu}^+\}$

where a spurion $\chi_\pm$ is introduced as

$$\chi = 2B_0\mathrm{diag}(m_u,m_d,m_s) = \mathrm{diag}(m_\pi^2,m_\pi^2,2m_K^2-m_\pi^2),$$
$$\chi_\pm = u^\dagger\chi u^\dagger \pm u\chi^\dagger u.$$

At the leading order,

$$\chi_+ = \mathrm{diag}(2m_\pi^2,2m_\pi^2,4m_K^2-2m_\pi^2),$$
$$\tilde{\chi}_+ = \chi_+ - \frac{1}{3}\mathrm{Tr}(\chi_+). \tag{30}$$

In principle, there should be six independent terms in Eq. (29) as the possible flavor structures listed in Table I. However, the terms $\mathrm{Tr}(\chi_+)$, $\mathrm{Tr}(f_{\mu\nu}^+)$ and $\mathrm{Tr}(\chi_+)\tilde{f}_{\mu\nu}^+$ can also be absorbed into Eq. (23) by renormalizing $\tilde{a}$ and a, respectively. Another term $[\tilde{\chi}_+,\tilde{f}_{\mu\nu}^+]$ vanishes since both $\tilde{\chi}_+$ and $\tilde{f}_{\mu\nu}^+$ are diagonal matrices at the leading order. Therefore, only three terms are retained in Eq. (29).

IV. RADIATIVE TRANSITIONS

A. Power counting and analytical expressions for the transition from factors

The standard power-counting scheme gives the chiral order of a Feynman diagram as

$$\mathcal{O} = 4N_L - 2I_M - I_H + \sum_n nN_n, \tag{31}$$

where N_L, I_M, and I_H are the numbers of loops, internal light pseudoscalar lines, and internal heavy meson lines, respectively. N_n is the number of vertices governed by the nth-order Lagrangians. Usually, the order of the (transition) magnetic moment is

$$\mathcal{O}_\mu = \mathcal{O} - 1. \tag{32}$$

Therefore, the transition form factors of $V\to P\gamma$ can be expressed as follows:

$$\mu'_{V\to P\gamma} = [\mu'^{(1)}_{\mathrm{tree}}] + [\mu'^{(2)}_{\mathrm{loop}}] + [\mu'^{(3)}_{\mathrm{tree}} + \mu'^{(3)}_{\mathrm{loop}}], \tag{33}$$

where the numbers in the parentheses are the chiral order $\mathcal{O}_\mu$.

We first study the $V\to P\gamma$ transitions. The tree diagrams are illustrated in Fig. 1. By expanding the Lagrangians in Eqs. (23) and (29), we can easily get the transition amplitudes of Figs. 1(a) and 1(b), respectively. We can extract the q^2-independent form factor μ' at the tree level by comparing the transition amplitudes with Eqs. (1) and (4). The expressions read

$$\mu'^{(a)}_{\bar{D}^{*0}\to\bar{D}^0\gamma} = \frac{16}{3}(\tilde{a}-3a), \tag{34}$$

$$\mu'^{(a)}_{D^{*-}\to D^-\gamma} = -\frac{8}{3}(\tilde{a}+6a), \tag{35}$$

$$\mu'^{(a)}_{D_s^{*-}\to D_s^-\gamma} = -\frac{8}{3}(\tilde{a}+6a), \tag{36}$$

$$\mu'^{(b)}_{\bar{D}^{*0}\to\bar{D}^0\gamma} = -\frac{32}{9}(m_K^2-m_\pi^2)(-6\tilde{d}+3\bar{d}+4d), \tag{37}$$

$$\mu'^{(b)}_{D^{*-}\to D^-\gamma} = -\frac{32}{9}(m_K^2-m_\pi^2)(-6\tilde{d}+3\bar{d}-2d), \tag{38}$$

$$\mu'^{(b)}_{D_s^{*-}\to D_s^-\gamma} = -\frac{32}{9}(m_K^2-m_\pi^2)(12\tilde{d}+3\bar{d}+4d). \tag{39}$$

We show the analytical expressions for the D mesons and display the expressions for the B mesons in Appendix A.

The one-loop Feynman diagrams that contribute to the transition processes are shown in Fig. 2. Here, we need to deal with the loop integrals when extracting the q^2-dependent form factors from the transition amplitudes. Various types of loop integrals $\mathcal{J}$ have been defined and given in Appendix B. In the following equations, we list the transition form factors of Figs. 2(a)–2(j) in a compact form, correspondingly:

$$\mu'^{(a)} = \sum_\phi \mathcal{C}_\phi^{(a)}\frac{g^2}{f_\phi^2}\{\mathcal{J}_{21}^T(m_\phi,\mathcal{E},q)\}_r, \tag{40}$$

$$\mu'^{(b)} = \sum_\phi \mathcal{C}_\phi^{(b)}\frac{\tilde{a}}{f_\phi^2}\{\mathcal{J}_0^c(m_\phi)\}_r, \tag{41}$$

FIG. 1. The diagrams for the $V\to P\gamma$ transitions at the tree level. The thick solid, thin solid, and wiggly lines represent the vector meson V, pseudoscalar meson P, and photon γ, respectively. The solid circle and solid square in diagrams (a) and (b) correspond to the $\mathcal{O}(p^2)$ and $\mathcal{O}(p^4)$ vertices, respectively.

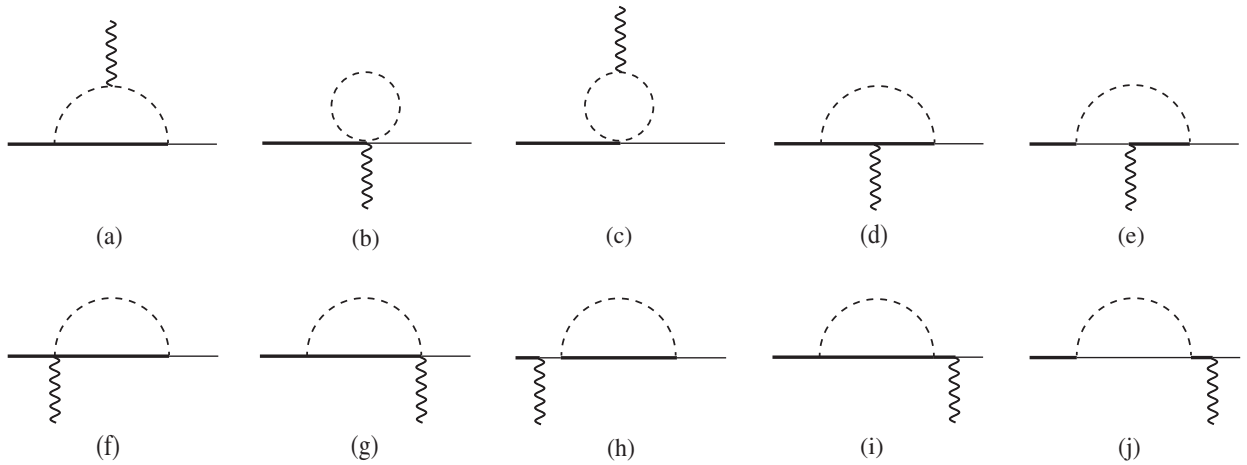

FIG. 2. The diagrams for the $V \to P\gamma$ transitions at the one-loop level, where the dashed line represents the light pseudoscalar mesons. Other notations are same as those in Fig. 1.

$$\mu'^{(c)} = \sum_\phi \mathcal{C}_\phi^{(c)} \frac{b}{f_\phi^2} \{\mathcal{J}_{22}^F(m_\phi, q)\}_r, \tag{42}$$

$$\mu'^{(d)} = \sum_\phi \mathcal{C}_\phi^{(d)} \frac{g^2}{f_\phi^2} \{\mathcal{J}_{22}^g(m_\phi, \mathcal{E}, \mathcal{E} - q_0)\}_r, \tag{43}$$

$$\mu'^{(e)} = \sum_\phi \mathcal{C}_\phi^{(e)} \frac{g^2}{f_\phi^2} \{\mathcal{J}_{22}^g(m_\phi, \mathcal{E} + \Delta, \mathcal{E} - q_0)\}_r, \tag{44}$$

$$\mu'^{(f)} = \mu^{(g)} = 0, \tag{45}$$

$$\mu'^{(h)} = \sum_\phi \mathcal{C}_\phi^{(h)} \frac{g^2}{f_\phi^2} \{(1-D)\partial_\omega \mathcal{J}_{22}^a(m_\phi, \omega)|_{\omega\to-\Delta}\}_r, \tag{46}$$

$$\mu'^{(i)+(j)} = \sum_\phi \mathcal{C}_\phi^{(ij)} \frac{g^2}{f_\phi^2} \left\{ [\partial_\omega \mathcal{J}_{22}^a(m_\phi, \omega) + 2\partial_\delta \mathcal{J}_{22}^a(m_\phi, \delta)] \Big|_{\omega\to\mathcal{E}+\Delta}^{\delta\to\mathcal{E}} \right\}_r, \tag{47}$$

where the summations over ϕ denote the possible contributions from the light pseudoscalars (ϕ could be π, K, η) in the loops. $\mathcal{C}_\phi^{(x)}(x = a, \ldots, j)$ are the flavor-dependent coefficients, and their values are given in Tables II and III. In the $\mathcal{J}$ functions, m_ϕ is the mass of the corresponding particle in the loop. $\mathcal{E}$ is the residual energy of heavy mesons, which is defined as $\mathcal{E} = E_{D^{(*)}} - m_{D^{(*)}}$. $\mathcal{E}$ is set to be zero in our calculations. q denotes the transferred momentum carried by the photon. D is the dimension in dimensional regularization. $\{X\}_r$ represents the finite part of X, which is defined in Appendix B. The coefficients $\mathcal{C}_\phi^{(ij)}$ can be obtained via the relation

$$\mathcal{C}_\phi^{(ij)} = -\mathcal{C}_\phi^{(h)}. \tag{48}$$

B. Estimation of the leading-order LECs

In $\mu_{\rm tree}'^{(1)}$, there exist two $\mathcal{O}(p^2)$ LECs, $\tilde{a}$ and a [see Eq. (23)]. Another $\mathcal{O}(p^2)$ LEC b [see Eq. (25)] resides in

TABLE II. The flavor-dependent coefficients $\mathcal{C}_\phi^{(x)}(x = a, \ldots, d)$ in Eqs. (40)–(43) for the $\bar{D}^*$ mesons.

Decay modes	$\mathcal{C}_\pi^{(a)}$	$\mathcal{C}_K^{(a)}$	$\mathcal{C}_\pi^{(b)}$	$\mathcal{C}_K^{(b)}$	$\mathcal{C}_\pi^{(c)}$	$\mathcal{C}_K^{(c)}$	$\mathcal{C}_\pi^{(d)}$	$\mathcal{C}_K^{(d)}$	$\mathcal{C}_\eta^{(d)}$
$\bar{D}^{*0} \to \bar{D}^0\gamma$	2	2	−4	−4	4	4	$24a$	$\frac{8}{3}(6a - \tilde{a})$	$\frac{8}{9}(3a + \tilde{a})$
$D^{*-} \to D^-\gamma$	−2	0	4	0	−4	0	$4(6a + \tilde{a})$	$\frac{8}{3}(6a - \tilde{a})$	$\frac{4}{9}(6a - \tilde{a})$
$D_s^{*-} \to D_s^-\gamma$	0	−2	0	4	0	−4	0	$\frac{8}{3}(12a + \tilde{a})$	$\frac{16}{9}(6a - \tilde{a})$

TABLE III. The flavor-dependent coefficients $\mathcal{C}_\phi^{(x)}(x = e, \ldots, j)$ in Eqs. (44)–(47) for the $\bar{D}^*$ mesons.

Decay modes	$\mathcal{C}_\pi^{(e)}$	$\mathcal{C}_K^{(e)}$	$\mathcal{C}_\eta^{(e)}$	$\mathcal{C}_\pi^{(h)}$	$\mathcal{C}_K^{(h)}$	$\mathcal{C}_\eta^{(h)}$
$\bar{D}^{*0} \to \bar{D}^0\gamma$	$12a$	$\frac{4}{3}(6a + \tilde{a})$	$\frac{4}{9}(3a - \tilde{a})$	$2(\tilde{a} - 3a)$	$\frac{4}{3}(\tilde{a} - 3a)$	$\frac{2}{9}(\tilde{a} - 3a)$
$D^{*-} \to D^-\gamma$	$2(6a - \tilde{a})$	$\frac{4}{3}(6a + \tilde{a})$	$\frac{2}{9}(6a + \tilde{a})$	$-(\tilde{a} + 6a)$	$-\frac{2}{3}(\tilde{a} + 6a)$	$-\frac{1}{9}(\tilde{a} + 6a)$
$D_s^{*-} \to D_s^-\gamma$	0	$\frac{4}{3}(12a - \tilde{a})$	$\frac{8}{9}(6a + \tilde{a})$	0	$-\frac{4}{3}(\tilde{a} + 6a)$	$-\frac{4}{9}(\tilde{a} + 6a)$

$\mu'^{(3)}_{\rm loop}$. In the following, we estimate the values of $\tilde{a}$, a, and b with the quark model and resonance saturation model, respectively. It is hard to determine the other higher-order LECs ($\tilde{d}$, $\bar{d}$, and d) in $\mu'^{(3)}_{\rm tree}$ for the moment because of very limited experimental data. Therefore, we consider the contributions from $\mu'^{(3)}_{\rm tree}$ as errors of our numerical results.

We first demonstrate how to determine $\tilde{a}$ and a from the scenario of a constituent quark model. In this model, the transition matrix element of $V \to P\gamma$ in the rest frame of the initial state can be written as [29]

$$\langle P|\mathcal{L}_{\rm em}|V\rangle = 2\sqrt{m_V m_P}\langle P|\sum_i \frac{e_i}{2m_i}\boldsymbol{\sigma}|V\rangle \cdot \mathbf{B}, \quad (49)$$

where e_i and m_i are the electric charge and mass of the ith quark in the heavy meson, and $\boldsymbol{\sigma}$ and $\mathbf{B}$ are the Pauli matrix and magnetic field, respectively. For simplicity, we choose the direction of the magnetic field $\mathbf{B}$ to be along the z axis. In order to work out Eq. (49), we need the flavor-spin wave functions of V and P, which read

$$|V\rangle = \frac{1}{\sqrt{2}}|\bar{Q}\uparrow q\downarrow + \bar{Q}\downarrow q\uparrow\rangle, \quad (50)$$

$$|P\rangle = \frac{1}{\sqrt{2}}|\bar{Q}\uparrow q\downarrow - \bar{Q}\downarrow q\uparrow\rangle. \quad (51)$$

Inserting Eqs. (50) and (51) into Eq. (49), one can obtain

$$\langle P|\mathcal{L}_{\rm em}|V\rangle = 2\sqrt{m_V m_P}(\mu_{\bar{Q}} - \mu_q), \quad (52)$$

where $\mu_i = e_i/(2m_i)$. Matching Eq. (52) with the leading-order transition amplitudes [i.e., replacing $\mu'(q^2)$ in Eq. (4) with the expressions in Eqs. (34)–(36), and making use of $B^k(\boldsymbol{q}) = -i\epsilon^{ijk}q^i A^j(\boldsymbol{q})$], one can easily get

$$\tilde{a} = -\frac{1}{8m_q}, \qquad a = \frac{1}{24m_{\bar{Q}}}, \quad (53)$$

where m_q and $m_{\bar{Q}}$ are the masses of the light constituent quark and the heavy antiquark in heavy mesons (in Appendix C, we also give an estimation of the light quark mass with the vector meson dominance model), respectively.

Next, we evaluate the value of LEC b in Eq. (25) using the resonance saturation model [55,56]. A diagrammatic presentation of the resonance saturation scheme is illustrated in Fig. 3. We need the interaction Lagrangians for $VP\rho$ and $\rho\pi\pi(\phi KK)$. The $VP\rho$ Lagrangian can be obtained with local hidden symmetry [31], which reads

$$\mathcal{L}_{H\rho} = i\beta\langle\bar{\mathcal{H}}v^\mu(\mathcal{V}_\mu - \rho_\mu)\mathcal{H}\rangle + i\lambda\langle\bar{\mathcal{H}}\sigma^{\mu\nu}F_{\mu\nu}(\rho)\mathcal{H}\rangle, \quad (54)$$

where

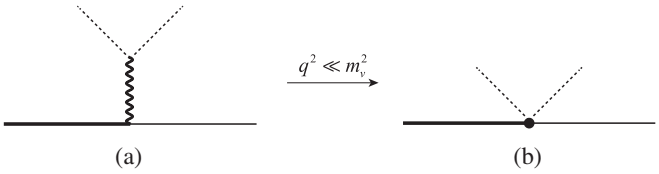

FIG. 3. A diagrammatic presentation of the resonance saturation scheme. The thick wiggly line in diagram (a) denotes the light vector meson ρ or ϕ, and other notations are same as those in Fig. 2.

$$F_{\mu\nu}(\rho) = \partial_\mu\rho_\nu - \partial_\nu\rho_\mu + [\rho_\mu, \rho_\nu], \qquad \rho_\mu = i\frac{g_v}{\sqrt{2}}\hat{\rho}_\mu \quad (55)$$

and

$$\hat{\rho}^\mu = \begin{pmatrix} \frac{\rho_0+\omega}{\sqrt{2}} & \rho^+ & K^{*+} \\ \rho^- & \frac{-\rho_0+\omega}{\sqrt{2}} & K^{*0} \\ K^{*-} & \bar{K}^{*0} & \phi \end{pmatrix}^\mu. \quad (56)$$

The $\rho\pi\pi(\phi KK)$ Lagrangian reads [31]

$$\mathcal{L}_{v\phi} = f_\phi^2 a{\rm Tr}(\Gamma_\mu^{(0)}\rho^\mu + \rho^\mu\Gamma_\mu^{(0)}), \quad a = 2, \quad (57)$$

where the expression of $\Gamma_\mu^{(0)}$ can be extracted from the chiral connection defined in Eq. (13) by omitting the photon field.

With the above preparations, we use the amplitude of Fig. 3(a) governed by the Lagrangians in Eqs. (54) and (57) to match the amplitude of Fig. 3(b) depicted by the Lagrangian in Eq. (25). We can get the b explicitly:

$$b = -\frac{2\lambda g_v^2 f_\phi^2}{m_v^2}, \quad (58)$$

where $g_v = 5.8$, $\lambda = 0.56\ {\rm GeV}^{-1}$ [57]. m_v is the mass of the exchanged light vector meson, such as $m_\rho = 0.77$ GeV and $m_\phi = 1.02$ GeV [9]. The sign of b is determined with the quark model.

The numerical values of the parameters are [9,36–38,52,53]

$$\begin{aligned} &m_\pi = 0.139\,{\rm GeV}, \quad m_K = 0.494\,{\rm GeV}, \quad m_\eta = 0.548\,{\rm GeV}, \\ &m_u = m_d = 0.336\,{\rm GeV}, \quad m_s = 0.54\,{\rm GeV}, \\ &m_c = 1.66\,{\rm GeV}, \quad m_b = 4.73\,{\rm GeV}, \\ &g = \begin{cases} 0.59 \pm 0.01 \pm 0.07 & \text{for } D^*D\pi \text{ coupling} \\ 0.516 \pm 0.05 \pm 0.033 & \text{for } B^*B\pi \text{ coupling} \end{cases}, \\ &\Delta = \begin{cases} 0.142\,{\rm GeV} & \text{for } m_{D^{*0}} - m_{D^0} \\ 0.045\,{\rm GeV} & \text{for } m_{B^{*0}} - m_{B^0} \end{cases}. \end{aligned} \quad (59)$$

Since the masses of the mesons have been precisely measured in experiments [9], we do not quote their minor

TABLE IV. The transition magnetic moments and magnetic moments of the charmed and bottom vector mesons calculated in the SU(2) case order by order (in units of μ_N).

	$\Delta = 0$				$\Delta \neq 0$			
Physical quantity	$\mathcal{O}_\mu(p^1)$ tree	$\mathcal{O}_\mu(p^2)$ loop	$\mathcal{O}_\mu(p^3)$ loop	Total	$\mathcal{O}_\mu(p^1)$ tree	$\mathcal{O}_\mu(p^2)$ loop	$\mathcal{O}_\mu(p^3)$ loop	Total
$\mu_{\bar{D}^{*0}\to\bar{D}^0\gamma}$	−2.24	0.21	−0.10	−2.13	−2.24	0.29	0.04	−1.91
$\mu_{D^{*-}\to D^-\gamma}$	0.55	−0.21	0.05	0.39	0.55	−0.29	0.02	0.28
$\mu_{B^{*+}\to B^+\gamma}$	−1.80	0.16	−0.09	−1.73	−1.80	0.19	−0.07	−1.68
$\mu_{B^{*0}\to B^0\gamma}$	0.99	−0.16	0.046	0.88	0.99	−0.19	0.04	0.84
$\mu_{\bar{D}^{*0}}$	1.48	−0.21	0.11	1.38	1.48	0.07	0.05	1.60
$\mu_{D^{*-}}$	−1.31	0.21	−0.05	−1.14	−1.31	−0.07	−0.007	−1.39
$\mu_{B^{*+}}$	1.93	−0.16	0.09	1.86	1.93	−0.13	0.09	1.90
$\mu_{B^{*0}}$	−0.86	0.16	−0.05	−0.75	−0.86	0.13	−0.05	−0.78

TABLE V. The transition magnetic moments and magnetic moments of charmed and bottom vector mesons calculated in the SU(3) case order by order (in units of μ_N).

	$\Delta = 0$				$\Delta \neq 0$			
Physical quantity	$\mathcal{O}_\mu(p^1)$ tree	$\mathcal{O}_\mu(p^2)$ loop	$\mathcal{O}_\mu(p^3)$ loop	Total	$\mathcal{O}_\mu(p^1)$ tree	$\mathcal{O}_\mu(p^2)$ loop	$\mathcal{O}_\mu(p^3)$ loop	Total
$\mu_{\bar{D}^{*0}\to\bar{D}^0\gamma}$	−2.24	0.71	−0.34	−1.86	−2.24	0.81	−0.13	−1.57
$\mu_{D^{*-}\to D^-\gamma}$	0.55	−0.21	0.19	0.54	0.55	−0.29	0.08	0.34
$\mu_{D_s^{*-}\to D_s^-\gamma}$	0.20	−0.50	0.15	−0.15	0.20	−0.51	0.10	−0.21
$\mu_{B^{*+}\to B^+\gamma}$	−1.80	0.55	−0.34	−1.58	−1.80	0.58	−0.30	−1.52
$\mu_{B^{*0}\to B^0\gamma}$	0.99	−0.16	0.17	1.0	0.99	−0.19	0.14	0.95
$\mu_{B_s^{*0}\to B_s^0\gamma}$	0.65	−0.39	0.13	0.38	0.65	−0.39	0.11	0.36
$\mu_{\bar{D}^{*0}}$	1.48	−0.71	0.40	1.18	1.48	−0.40	0.40	1.48
$\mu_{D^{*-}}$	−1.31	0.21	−0.21	−1.31	−1.31	−0.07	−0.24	−1.62
$\mu_{D_s^{*-}}$	−0.96	0.50	−0.16	−0.62	−0.96	0.47	−0.21	−0.69
$\mu_{B^{*+}}$	1.93	−0.55	0.34	1.71	1.93	−0.52	0.36	1.77
$\mu_{B^{*0}}$	−0.86	0.16	−0.17	−0.87	−0.86	0.13	−0.19	−0.92
$\mu_{B_s^{*0}}$	−0.51	0.39	−0.13	−0.25	−0.51	0.38	−0.14	−0.27

errors. The masses of the constituent quarks are adopted from previous works [36–38]. Generally, it is hard to give the errors of the masses of the constituent quarks, because these values used in different quark models vary a lot. In this work, we try to give a conservative estimation by setting $10\% \times m_q$ as the parameter errors. The axial constant g for the $D^*D\pi$ coupling is extracted from the experimental result of the CLEO Collaboration [52]. The $B^*B\pi$ coupling is quoted from the unquenched lattice result [53].

C. Numerical results and discussions

With the parameters listed above, we first show the transition magnetic moments of $V \to P\gamma$ calculated under the SU(2) and SU(3) symmetries[2] in the upper-half parts of Tables IV and V, correspondingly. In Tables IV and V, the transition magnetic moments $\mu_{V\to P\gamma}$ are given order by order. As expected, the convergence of the chiral expansion in the SU(2) case is better than that in SU(3). Besides, we also calculate the $\mu_{V\to P\gamma}$ with the mass splitting Δ in the propagators of the loop diagrams both kept and unkept. The influence of Δ in the charm sector is more significant than that in the bottom sector, because the mass difference of the charmed mesons is larger than that of the bottom mesons.

In the SU(2) case, the mass splitting Δ only appears in the loop diagrams. The transition magnetic moments at $\mathcal{O}_\mu(p^1)$ remain unchanged no matter if we choose $\Delta = 0$ or $\Delta \neq 0$. At $\mathcal{O}_\mu(p^2)$, the correction from the finite mass splitting ($\Delta \neq 0$) is about 40% and 20% for $\mu_{\bar{D}^*\to\bar{D}\gamma}$ and $\mu_{B^*\to B\gamma}$, respectively. Such a correction is also significant at $\mathcal{O}_\mu(p^3)$. Similar behavior is observed in the SU(3) case at each order. In Table VI, we show the contribution of each loop diagram to the transition magnetic moment of $\bar{D}^{*0} \to \bar{D}\gamma$ in different cases. The contributions of the diagrams in Figs. 2(f) and 2(g) vanish in the heavy quark limit. Except

[2]Here, SU(2) and SU(3) symmetries only imply that the effective Lagrangians are constructed under these two symmetries. The SU(3) breaking effect is included explicitly in our calculations. For example, we use $m_{u,d,s}$ and the physical masses of π, K, and η in Eq. (59) as inputs.

TABLE VI. The contribution of each loop diagram to the transition magnetic moment of $\bar{D}^{*0} \to \bar{D}\gamma$ in different cases (in units of μ_N).

Cases		(a)	(b)	(c)	(d)	(e)	(f)	(g)	(h)	$(i+j)$
SU(2)	$\Delta = 0$	0.21	−0.085	0.062	0.012	0.006	0	0	−0.045	−0.053
	$\Delta \neq 0$	0.29	−0.085	0.062	−0.0016	0.0021	0	0	0.073	−0.0082
SU(3)	$\Delta = 0$	0.71	−0.37	0.27	0.088	−0.00017	0	0	−0.13	−0.19
	$\Delta \neq 0$	0.81	−0.37	0.27	0.033	−0.0038	0	0	0.13	−0.19

for the diagrams in Figs. 2(b) and 2(c), other diagrams that contain the heavy meson internal line are affected by the mass splitting Δ. For the charmed vector mesons, $\Delta > m_\pi$, so the loop integrals with the nonanalytic structures $\log\frac{y^2+m_\pi^2-\Delta^2-i\varepsilon}{\lambda^2}$ and $\sqrt{m_\pi^2-\Delta^2-i\varepsilon}$ (see Appendix B) would largely impact the numerical result. This is vividly reflected in Table VI. However, for the bottom vector mesons, $\Delta \simeq 1/3 m_\pi$, so the influence of Δ on the bottom sector is not so obvious.

The corresponding decay widths evaluated in different cases are illustrated in Table VIII. The errors in our calculations can stem from many sources, such as quark masses, hadron masses, coupling constants, higher-order contributions, and so on. As shown in Ref. [9], the errors of the hadron masses that appear in this work are very small, so we ignore their effects. Meanwhile, the axial coupling constant extracted from the experiments and lattice QCD are also very small. Furthermore, the convergence of chiral expansion works very well in our calculations. Therefore, we consider two main error sources. The first one is the contribution of the $\mathcal{O}(p^4)$ Lagrangians [see Eq. (29)]. Since the LECs in Eq. (29) cannot be fixed at present, we adopt the nonanalytic dominance approximation to give an estimation of the $\mathcal{O}(p^4)$ tree diagram [58]. The second one is the uncertainty from the quark models. For example, the masses of constituent quarks are different in various models (see Table VII). We take this uncertainty into account. The change of the quark masses would lead to a 10% variation of the leading-order LECs.

TABLE VII. The masses of the constituent quarks adopted in different works (in units of GeV).

	m_u	m_d	m_s	m_c	m_b
Kamal [11]	0.34	0.34	0.55	1.8	⋯
Ebert [19]	0.33	0.33	0.5	1.55	4.88
Cheng [29]	0.338	0.322	0.51	1.6	5.0
Eichten [59]	0.335	0.335	0.45	1.84	5.17

From Table VIII, we see that the decay rate for $D^{*-} \to D^-\gamma$ calculated in different scenarios agrees with the experimental data. The branching ratios for the other decay channels cannot be obtained due to the absence of the total widths of these states in experiments at present. We also compare our results with other model predictions, such as the light-front quark model [14], the relativistic independent quark model [15], the relativistic quark model [19] and the QCD sum rules [25]. The results in these literatures are consistent with our calculations. Furthermore, the results from the extended Bag model [21,22], lattice QCD simulations [26], and extended Nambu-Jona-Lasinio model [32] are also compatible with ours.

Up to now, only the full width of $D^{*\pm}$ and the branching ratio of $D^{*\pm} \to D^\pm\gamma$ were available in Ref. [9]. The lifetime of $\bar{D}^{*0}$ and D_s^{*-} has not been measured yet. The convergence of the chiral expansion for transition magnetic moments calculated in the SU(3) case with $\Delta \neq 0$ is very reasonable. Therefore, as a byproduct, we use the following relation with our results in SU(3) and $\Delta \neq 0$ as inputs to estimate the full widths of these two states:

TABLE VIII. The radiative decay widths for $V \to P\gamma$ (in units of keV). $\mathrm{Br}_{\mathrm{expt}}$ and Γ_{expt} denote the branching ratio and decay width measured in experiments. $\Gamma_{1,\ldots,4}$ are the model predictions.

	SU(2)		SU(3)		Experimental data and model predictions				
Decay modes	$\Delta = 0$	$\Delta \neq 0$	$\Delta = 0$	$\Delta \neq 0$	$\mathrm{Br}_{\mathrm{expt}}\|\Gamma_{\mathrm{expt}}$ [9]	Γ_1 [14]	Γ_2 [15]	Γ_3 [19]	Γ_4 [25]
$\bar{D}^{*0} \to \bar{D}^0\gamma$	$30.0^{+7.3}_{-6.6}$	$23.9^{+5.0}_{-6.3}$	$22.9^{+8.2}_{-7.0}$	$16.2^{+6.5}_{-6.0}$	$(38.1 \pm 2.9)\%\|\cdots$	20.0 ± 0.3	26.5	11.5	12.9 ± 2
$D^{*-} \to D^-\gamma$	$1.0^{+0.9}_{-0.6}$	$0.5^{+0.5}_{-0.4}$	$1.8^{+1.3}_{-0.9}$	$0.73^{+0.7}_{-0.3}$	$(1.6 \pm 0.4)\%\|1.33 \pm 0.33$	0.9 ± 0.02	0.93	1.04	0.23 ± 0.1
$D_s^{*-} \to D_s^-\gamma$	⋯	⋯	$0.15^{+0.5}_{-0.1}$	$0.32^{+0.3}_{-0.3}$	$(94.2 \pm 0.7)\%\|\cdots$	0.18 ± 0.01	0.21	0.19	0.13 ± 0.05
$B^{*+} \to B^+\gamma$	$0.75^{+0.2}_{-0.2}$	$0.71^{+0.2}_{-0.2}$	$0.63^{+0.2}_{-0.2}$	$0.58^{+0.2}_{-0.2}$	$\cdots\|\cdots$	0.4 ± 0.03	0.58	0.19	0.13 ± 0.03
$B^{*0} \to B^0\gamma$	$0.19^{+0.05}_{-0.05}$	$0.18^{+0.05}_{-0.05}$	$0.25^{+0.06}_{-0.06}$	$0.23^{+0.06}_{-0.06}$	$\cdots\|\cdots$	0.13 ± 0.01	0.18	0.07	0.38 ± 0.06
$B_s^{*0} \to B_s^0\gamma$	⋯	⋯	$0.05^{+0.03}_{-0.03}$	$0.04^{+0.03}_{-0.03}$	$\cdots\|\cdots$	0.068 ± 0.017	0.12	0.05	0.22 ± 0.04

FIG. 4. Tree-level Feynman diagrams that contribute to the magnetic moments of the heavy vector mesons. Notations are same as those in Fig. 1.

$$\frac{\mathrm{Br}(D^{*\pm}\to D^{\pm}\gamma)_{\mathrm{expt}}}{\mathrm{Br}(\bar{D}^{*0}\to \bar{D}^{0}\gamma)_{\mathrm{expt}}}=\frac{\Gamma(D^{*\pm}\to D^{\pm}\gamma)}{\Gamma(\bar{D}^{*0}\to \bar{D}^{0}\gamma)}\frac{\Gamma_{\mathrm{tot}}(\bar{D}^{*0})}{\Gamma_{\mathrm{tot}}(D^{*\pm})}, \tag{60}$$

where the total width $\Gamma_{\mathrm{tot}}(\bar{D}^{*0})$ in the above equation can be extracted with the predicted $\Gamma(\bar{D}^{*0}\to\bar{D}^{0}\gamma)$. Analogously, $\Gamma_{\mathrm{tot}}(D_s^{*\pm})$ can also be calculated the same way as in the case of $\bar{D}^{*0}$. The full widths of $\bar{D}^{*0}$ and D_s^{*-} are estimated to be

$$\Gamma_{\mathrm{tot}}(\bar{D}^{*0})\simeq 77.7^{+26.7}_{-20.5}\ \mathrm{keV},\quad \Gamma_{\mathrm{tot}}(D_s^{*-})\simeq 0.62^{+0.45}_{-0.50}\ \mathrm{keV}, \tag{61}$$

respectively.

V. MAGNETIC MOMENTS

The anomalous magnetic moments of nucleons reveal that the proton and neutron are not elementary particles, and they have internal substructures. As in the case of nucleons, the magnetic moments of D^* and B^* also encode important information about their underlying substructures.

A. Analytical expressions for the magnetic moments

We have studied the radiative transitions $V\to P\gamma$ in the previous section. The decay rate for $D^{*-}\to D^{-}\gamma$ is consistent with the experimental data. So we adopt the same set of parameters to calculate the magnetic moments of the D^* and B^* mesons. The $\mathcal{O}(p^2)$ and $\mathcal{O}(p^4)$ tree-level Feynman diagrams that contribute to the magnetic moments are displayed in Fig. 4.

In the following, we write out the magnetic moments of the D^* mesons from Figs. 4(a) and 4(b):

$$\mu^{(a)}_{\bar{D}^{*0}}=-\frac{8}{3}e(\tilde{a}+3a), \tag{62}$$

$$\mu^{(a)}_{D^{*-}}=-\frac{4}{3}e(-\tilde{a}+6a), \tag{63}$$

$$\mu^{(a)}_{D_s^{*-}}=-\frac{4}{3}e(-\tilde{a}+6a), \tag{64}$$

$$\mu^{(b)}_{\bar{D}^{*0}}=\frac{16}{9}e(m_K^2-m_\pi^2)(6\tilde{d}+3\bar{d}+4d), \tag{65}$$

$$\mu^{(b)}_{D^{*-}}=\frac{16}{9}e(m_K^2-m_\pi^2)(6\tilde{d}+3\bar{d}-2d), \tag{66}$$

$$\mu^{(b)}_{D_s^{*-}}=\frac{16}{9}e(m_K^2-m_\pi^2)(-12\tilde{d}+3\bar{d}+4d). \tag{67}$$

The magnetic moments from the one-loop diagrams in Fig. 5 are given as

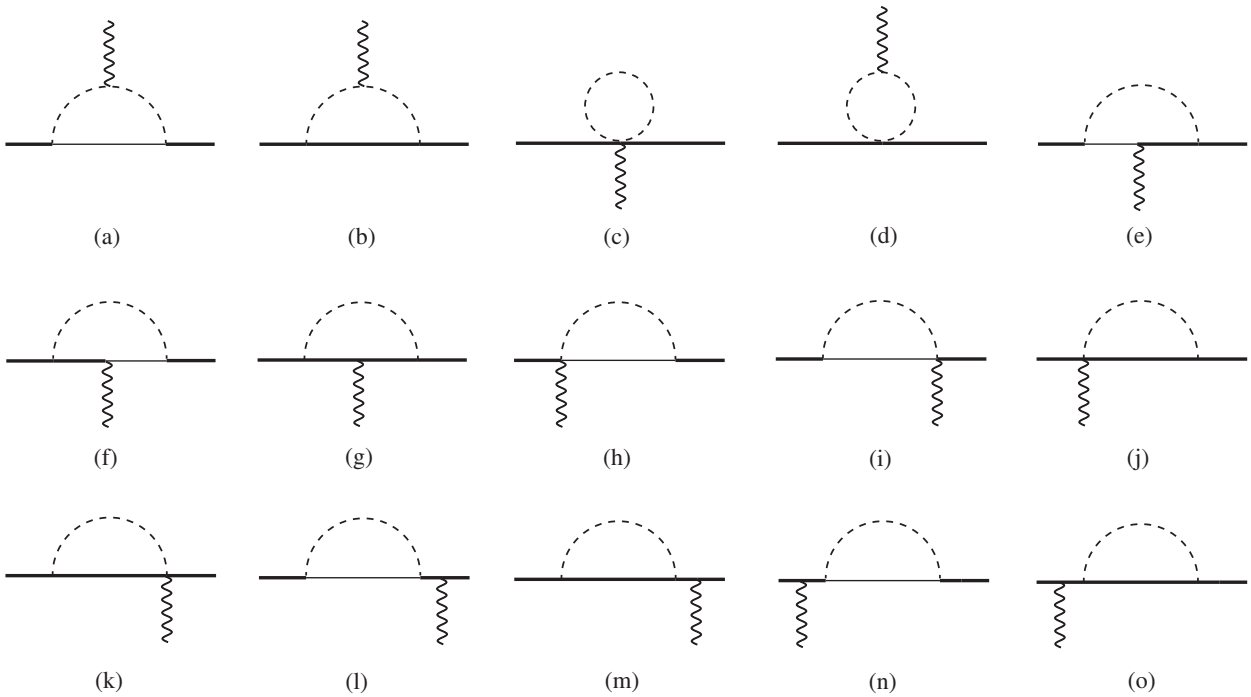

FIG. 5. One-loop Feynman diagrams that contribute to the magnetic moments of the heavy vector mesons. Notations are the same as those in Fig. 2.

TABLE IX. The flavor-dependent coefficients $\mathcal{C}_\phi^{(x)}(x=a,c,d,e)$ in Eqs. (68)–(72) for the $\bar{D}^*$ mesons.

States	$\mathcal{C}_\pi^{(a)}$	$\mathcal{C}_K^{(a)}$	$\mathcal{C}_\pi^{(c)}$	$\mathcal{C}_K^{(c)}$	$\mathcal{C}_\pi^{(d)}$	$\mathcal{C}_K^{(d)}$	$\mathcal{C}_\pi^{(e)}$	$\mathcal{C}_K^{(e)}$	$\mathcal{C}_\eta^{(e)}$
$\bar{D}^{*0}$	$-\frac{1}{2}$	$-\frac{1}{2}$	2	2	-2	-2	$6a$	$\frac{2}{3}(6a+\tilde{a})$	$\frac{2}{9}(3a-\tilde{a})$
D^{*-}	$\frac{1}{2}$	0	-2	0	2	0	$6a-\tilde{a}$	$\frac{2}{3}(6a+\tilde{a})$	$\frac{1}{9}(6a+\tilde{a})$
D_s^{*-}	0	$\frac{1}{2}$	0	-2	0	2	0	$\frac{2}{3}(12a-\tilde{a})$	$\frac{4}{9}(6a+\tilde{a})$

TABLE X. The flavor-dependent coefficients $\mathcal{C}_\phi^{(x)}(x=g,l+m)$ in Eqs. (74)–(76) for the $\bar{D}^*$ mesons.

States	$\mathcal{C}_\pi^{(g)}$	$\mathcal{C}_K^{(g)}$	$\mathcal{C}_\eta^{(g)}$	$\mathcal{C}_\pi^{(lm)}$	$\mathcal{C}_K^{(lm)}$	$\mathcal{C}_\eta^{(lm)}$
$\bar{D}^{*0}$	$6a$	$\frac{2}{3}(6a-\tilde{a})$	$\frac{2}{9}(3a+\tilde{a})$	$(\tilde{a}+3a)$	$\frac{2}{3}(\tilde{a}+3a)$	$\frac{1}{9}(\tilde{a}+3a)$
D^{*-}	$6a+\tilde{a}$	$\frac{2}{3}(6a-\tilde{a})$	$\frac{1}{9}(6a-\tilde{a})$	$\frac{1}{2}(6a-\tilde{a})$	$\frac{1}{3}(6a-\tilde{a})$	$\frac{1}{18}(6a-\tilde{a})$
D_s^{*-}	0	$\frac{2}{3}(12a+\tilde{a})$	$\frac{4}{9}(6a-\tilde{a})$	0	$\frac{2}{3}(6a-\tilde{a})$	$\frac{2}{9}(6a-\tilde{a})$

$$\mu^{(a)}=\sum_\phi e\mathcal{C}_\phi^{(a)}\frac{g^2}{f_\phi^2}\mathcal{J}_{21}^T(m_\phi,\mathcal{E}+\Delta,q), \tag{68}$$

$$\mu^{(b)}=\sum_\phi e\mathcal{C}_\phi^{(b)}\frac{g^2}{f_\phi^2}\mathcal{J}_{21}^T(m_\phi,\mathcal{E},q), \tag{69}$$

$$\mu^{(c)}=\sum_\phi e\mathcal{C}_\phi^{(c)}\frac{\tilde{a}}{f_\phi^2}\mathcal{J}_0^c(m_\phi), \tag{70}$$

$$\mu^{(d)}=\sum_\phi e\mathcal{C}_\phi^{(d)}\frac{b}{f_\phi^2}\mathcal{J}_{22}^F(m_\phi,q), \tag{71}$$

$$\mu^{(e)}=\sum_\phi e\mathcal{C}_\phi^{(e)}\frac{g^2}{f_\phi^2}\mathcal{J}_{22}^g(m_\phi,\mathcal{E}+\Delta,\mathcal{E}-q_0), \tag{72}$$

$$\mu^{(f)}=\sum_\phi e\mathcal{C}_\phi^{(f)}\frac{g^2}{f_\phi^2}\mathcal{J}_{22}^g(m_\phi,\mathcal{E},\mathcal{E}+\Delta-q_0), \tag{73}$$

$$\mu^{(g)}=\sum_\phi e\mathcal{C}_\phi^{(g)}\frac{g^2}{f_\phi^2}\mathcal{J}_{22}^g(m_\phi,\mathcal{E},\mathcal{E}-q_0), \tag{74}$$

$$\mu^{(h)}=\mu^{(i)}=\mu^{(j)}=\mu^{(k)}=0, \tag{75}$$

$$\mu^{(l)+(m)}=\mu^{(n)+(o)}=\sum_\phi e\mathcal{C}_\phi^{(lm)}\frac{g^2}{f_\phi^2}\{[\partial_\omega\mathcal{J}_{22}^a(m_\phi,\omega)+2\partial_\delta\mathcal{J}_{22}^a(m_\phi,\delta)]|_{\omega\to\mathcal{E}+\Delta}^{\delta\to\mathcal{E}}\}_r, \tag{76}$$

where the values of the coefficients $\mathcal{C}_\phi^{(x)}(x=a,\ldots,o)$ for the D^* mesons are listed in Tables IX and X. In Eqs. (68) and (69), we have used the relation $\mathcal{J}_{31}^T=-\frac{1}{2}\mathcal{J}_{21}^T$ when $q^2=0$ [58]. The unlisted coefficients $\mathcal{C}_\phi^{(b)}$ and $\mathcal{C}_\phi^{(f)}$ can be obtained by the relation

$$\mathcal{C}_\phi^{(b)}=\mathcal{C}_\phi^{(a)},\qquad \mathcal{C}_\phi^{(f)}=\mathcal{C}_\phi^{(e)}. \tag{77}$$

Analogously to the transition form factors $\mu'_{V\to P\gamma}$ in Eq. (33), the magnetic moments μ_V can be written as

$$\mu_V=[\mu_{\rm tree}^{(1)}]+[\mu_{\rm loop}^{(2)}]+[\mu_{\rm tree}^{(3)}+\mu_{\rm loop}^{(3)}], \tag{78}$$

where $\mu_{\rm tree}^{(1)}$, $\mu_{\rm loop}^{(2)}$, and $\mu_{\rm loop}^{(3)}$ can be calculated by using the parameters in Eq. (59) as inputs.

B. Numerical results and discussions

The numerical results for the magnetic moments μ_V calculated in the SU(2) and SU(3) cases are given order by order in the lower-half parts of Tables IV and V, respectively. We see that the convergence of the chiral expansion in the SU(2) case remains very good, and the convergence is also reasonable in SU(3).

In the SU(2) case, the magnetic moments at $\mathcal{O}_\mu(p^1)$ are independent of Δ. The $\Delta\neq 0$ correction reduces μ_V at $\mathcal{O}_\mu(p^2)$ and $\mathcal{O}_\mu(p^3)$. Consequently, the total results are increased. In the heavy quark limit, there exists a strict relationship between μ_V and $\mu_{V\to P\gamma}$ at each order; i.e., $|\mu_V|=|\mu_{V\to P\gamma}|$ when we take $D=4$ and $\Delta=0$ in the loop functions. Both the radiative transitions and magnetic moments of the heavy vector mesons are solely governed by the light quark, since the heavy quark decouples completely.

In the SU(3) case, one notices a similar variation trend at $\mathcal{O}_\mu(p^2)$ as in SU(2). At $\mathcal{O}_\mu(p^3)$, there is a moderate increase when the mass splitting is included. The total results are enhanced in the $\Delta\neq 0$ case. It is interesting to diagnose the convergence of the chiral expansion for magnetic moments from a straightforward dimensional analysis.

TABLE XI. The magnetic moments of the charmed and bottom vector mesons (in units of nucleon magnetons μ_N), and a comparison with the bag model (Bag), extended Nambu–Jona-Lasinio model (NJL) and extended bag model (Extended Bag) predictions.

	SU(2)		SU(3)		The results from other theoretical works		
States	$\Delta = 0$	$\Delta \neq 0$	$\Delta = 0$	$\Delta \neq 0$	Bag [20]	NJL [33]	Extended Bag [22]
$\bar{D}^{*0}$	$1.38^{+0.25}_{-0.25}$	$1.60^{+0.25}_{-0.25}$	$1.18^{+0.25}_{-0.25}$	$1.48^{+0.22}_{-0.38}$	0.89	⋯	1.28
D^{*-}	$-1.14^{+0.15}_{-0.15}$	$-1.39^{+0.15}_{-0.15}$	$-1.31^{+0.20}_{-0.15}$	$-1.62^{+0.24}_{-0.08}$	−1.17	−1.16	−1.13
D_s^{*-}	⋯	⋯	$-0.62^{+0.15}_{-0.15}$	$-0.69^{+0.22}_{-0.10}$	−1.03	−0.98	−0.93
B^{*+}	$1.86^{+0.25}_{-0.25}$	$1.90^{+0.20}_{-0.20}$	$1.71^{+0.25}_{-0.25}$	$1.77^{+0.25}_{-0.30}$	1.54	1.47	1.56
B^{*0}	$-0.75^{+0.11}_{-0.11}$	$-0.78^{+0.11}_{-0.11}$	$-0.87^{+0.13}_{-0.11}$	$-0.92^{+0.15}_{-0.11}$	−0.64	⋯	−0.69
B_s^{*0}	⋯	⋯	$-0.25^{+0.11}_{-0.11}$	$-0.27^{+0.13}_{-0.10}$	−0.47	⋯	−0.51

The magnetic moments μ_V at leading order (LO), next-to-leading order (NLO), and next-to-next-to-leading order (NNLO) can be parametrized as follows:

$$\begin{aligned} \text{LO}&: A\frac{1}{m_q} + B\frac{1}{m_Q}, \\ \text{NLO}&: C\frac{m_\phi}{\Lambda_\chi^2}, \\ \text{NNLO}&: \left(D\frac{1}{m_q} + E\frac{1}{m_Q}\right) \times \frac{m_\phi^2}{\Lambda_\chi^2}, \end{aligned} \tag{79}$$

where the coefficients $A, \ldots, E$ are order-one dimensionless constants. $\Lambda_\chi \sim 1$ GeV denotes the chiral breaking scale.

For the D^{*-} and B^{*0} mesons, the internal light pseudoscalar lines in the $\mathcal{O}(p^3)$ loop diagrams [Figs. 5(a) and 5(b)] can only be the charged pions. But for the $\mathcal{O}(p^4)$ wave function renormalization diagrams [Figs. 5(l)–5(o)], K and η would contribute to the loops. Since $m_K/m_\pi \simeq 3.5$ and $m_\eta/m_\pi \simeq 4.0$, the $\mathcal{O}(p^4)$ contribution would be enhanced to the same magnitude as the $\mathcal{O}(p^3)$ correction from the SU(3) violation effect. Let us take the D^{*-} meson as an example. In the strict heavy quark limit, the contributions of Figs. 5(a) and 5(b) are equal. However, for the charmed mesons, the mass splitting $\Delta > m_\pi$. Hence, the amplitudes of Figs. 5(a) and 5(b) are of similar size but with opposite signs, which makes the contributions of these two diagrams for D^{*-} largely cancel with each other. This effect does not contribute to the transition magnetic moments, because there is only a single one-loop diagram with $\Delta = 0$ at $\mathcal{O}(p^3)$ level [see Fig. 2(a)]. Moreover, the influence of the mass splitting on the magnetic properties of the B^* meson is not obvious due to $\Delta \ll m_\phi$ in the bottom sector.

The magnetic moments for the $\bar{D}^*$ and B^* mesons calculated in different cases are shown in Table XI, where the errors also stem from $\mu_{\text{tree}}^{(3)}$, i.e., $\mathcal{O}(p^4)$ Lagrangians and quark models. The magnetic moments of the vector $\bar{Q}u$, $\bar{Q}d$, and $\bar{Q}s$ states given by the bag model [20,22] and the Nambu–Jona-Lasinio model [33] are compatible with our predictions.

VI. SUMMARY

For the ground vector $\bar{Q}q$ states, heavy quark spin symmetry implies that the mass splitting between the spin triplets V and the spin singlets P is very small, of the same order as the pion mass m_π. Thus, the decay modes of V are largely restricted. For the ground-state charmed vector mesons, the dominant decay channels are $V \to P\pi$ and $V \to P\gamma$. For the $b\bar{q}$ states, the only dominant decay modes are $V \to P\gamma$.

In this work, we calculate the decay rates of $V \to P\gamma$ for the charmed and bottom vector mesons. Our result for $D^{*-} \to D^-\gamma$ is in accordance with the experimental measurement. We also investigate the convergence of the chiral expansion of the transition magnetic moments in the SU(2) and SU(3) cases with the mass splitting both kept and unkept. The results indicate that the convergence in the SU(2) case is very good, and it is likewise reasonable for SU(3). The effect of the mass splitting for the charmed mesons is more significant than that for the bottom mesons. The radiative decay widths of the D^* and B^* mesons from other theoretical models and lattice QCD simulations also are consistent with ours. As a byproduct, the full widths of $\bar{D}^{*0}$ and D_s^{*-} are estimated to be $77.7^{+26.7}_{-20.5}$ keV and $0.62^{+0.45}_{-0.50}$ keV, respectively.

In this work, we also calculate the magnetic moments of the D^* and B^* mesons. Our results agree with the predictions of the bag model [20,22] and the NJL model [33]. The magnetic moments of heavy vector mesons are good platforms to probe their inner structures. For example, the magnetic moment of $\bar{D}^{*0}$ should be zero if we use the classical formula $\boldsymbol{\mu} = \frac{e}{2m}\mathbf{S}$ (where e, m, and $\mathbf{S}$ denote the charge, mass, and spin, respectively). The large anomalous magnetic moment of $\bar{D}^{*0}$ clearly demonstrates that it is not a point particle.

In summary, we have systematically studied the radiative transitions and magnetic moments of charmed and bottom vector mesons with χPT up to $\mathcal{O}(p^4)$. Our numerical results are presented up to this order with different scenarios. The LECs $\tilde{a}$, a and b in the $\mathcal{O}(p^2)$ Lagrangians are estimated with

the quark model and the resonance saturation model, respectively. We notice that the one-loop chiral correction plays a very important role in mediating the (transition) magnetic moments. Our result indicates that the quark model prediction is not enough to describe the magnetic properties of the charmed and bottom vector mesons. The quark dynamics of the light degree of freedom that is related with the spontaneous breaking of chiral symmetry is non-negligible.

The present investigations of the radiative decays of D^* and B^* shall be helpful for future measurements at facilities such as Belle II and LHCb. Furthermore, the analytical expressions derived in χPT shall be helpful for the chiral extrapolations of lattice QCD simulations on the electromagnetic transitions and magnetic moments of heavy vector mesons.

ACKNOWLEDGMENTS

B. W. is very grateful to X. L. Chen and W. Z. Deng for helpful discussions. This project is supported by the National Natural Science Foundation of China under Grants No. 11575008 and No. 11621131001 and the National Key Basic Research Program of China (No. 2015CB856700).

APPENDIX A: SOME SUPPLEMENTAL MATERIALS FOR THE B^* MESONS

The transition form factors from Figs. 1(a) and 1(b) for the B^* mesons read

$$\mu^{\prime(a)}_{B^{*+}\to B^+\gamma} = \frac{8}{3}(3a+2\tilde{a}), \tag{A1}$$

$$\mu^{\prime(a)}_{B^{*0}\to B^0\gamma} = \frac{8}{3}(3a-\tilde{a}), \tag{A2}$$

$$\mu^{\prime(a)}_{B^{*0}_s\to B^0_s\gamma} = \frac{8}{3}(3a-\tilde{a}), \tag{A3}$$

$$\mu^{\prime(b)}_{B^{*+}\to B^+\gamma} = -\frac{32}{9}(m_K^2-m_\pi^2)(3\tilde{d}+3\bar{d}+4d), \tag{A4}$$

$$\mu^{\prime(b)}_{B^{*0}\to B^0\gamma} = -\frac{32}{9}(m_K^2-m_\pi^2)(3\tilde{d}+3\bar{d}-2d), \tag{A5}$$

$$\mu^{\prime(b)}_{B^{*0}_s\to B^0_s\gamma} = -\frac{32}{9}(m_K^2-m_\pi^2)(-6\tilde{d}+3\bar{d}+4d). \tag{A6}$$

The magnetic moments from Figs. 4(a) and 4(b) for the B^* mesons read

$$\mu^{(a)}_{B^{*+}} = \frac{4}{3}e(-2\tilde{a}+3a), \tag{A7}$$

$$\mu^{(a)}_{B^{*0}} = \frac{4}{3}e(\tilde{a}+3a), \tag{A8}$$

$$\mu^{(a)}_{B^{*0}_s} = \frac{8}{3}e(\tilde{a}+3a), \tag{A9}$$

$$\mu^{(b)}_{B^{*+}} = \frac{16}{9}e(m_K^2-m_\pi^2)(-3\tilde{d}+3\bar{d}+4d), \tag{A10}$$

$$\mu^{(b)}_{B^{*0}} = \frac{16}{9}e(m_K^2-m_\pi^2)(-3\tilde{d}+3\bar{d}-2d), \tag{A11}$$

$$\mu^{(b)}_{B^{*0}_s} = \frac{16}{9}e(m_K^2-m_\pi^2)(6\tilde{d}+3\bar{d}+4d). \tag{A12}$$

The flavor-dependent coefficients $\mathcal{C}^{(x)}_\phi$ in Eqs. (40)–(47) and Eqs. (68)–(76) for the B^* mesons are listed in Tables XII and XIII and Tables XIV and XV, respectively.

TABLE XII. The flavor-dependent coefficients $\mathcal{C}^{(x)}_\phi (x = a, \ldots, d)$ in Eqs. (40)–(43) for the B^* mesons.

Decay modes	$\mathcal{C}^{(a)}_\pi$	$\mathcal{C}^{(a)}_K$	$\mathcal{C}^{(b)}_\pi$	$\mathcal{C}^{(b)}_K$	$\mathcal{C}^{(c)}_\pi$	$\mathcal{C}^{(c)}_K$	$\mathcal{C}^{(d)}_\pi$	$\mathcal{C}^{(d)}_K$	$\mathcal{C}^{(d)}_\eta$
$B^{*+}\to B^+\gamma$	2	2	−4	−4	4	4	$-12a$	$-\frac{8}{3}(3a+\tilde{a})$	$-\frac{4}{9}(3a-2\tilde{a})$
$B^{*0}\to B^0\gamma$	−2	0	4	0	−4	0	$-4(3a-\tilde{a})$	$-\frac{8}{3}(3a+\tilde{a})$	$-\frac{4}{9}(3a+\tilde{a})$
$B^{*0}_s\to B^0_s\gamma$	0	−2	0	4	0	−4	0	$-\frac{8}{3}(6a-\tilde{a})$	$-\frac{16}{9}(3a+\tilde{a})$

TABLE XIII. The flavor-dependent coefficients $\mathcal{C}^{(x)}_\phi (x = e, \ldots, j)$ in Eqs. (44)–(47) for the B^* mesons.

Decay modes	$\mathcal{C}^{(e)}_\pi$	$\mathcal{C}^{(e)}_K$	$\mathcal{C}^{(e)}_\eta$	$\mathcal{C}^{(h)}_\pi$	$\mathcal{C}^{(h)}_K$	$\mathcal{C}^{(h)}_\eta$
$B^{*+}\to B^+\gamma$	$-6a$	$-\frac{4}{3}(3a-\tilde{a})$	$-\frac{2}{9}(3a+2\tilde{a})$	$3a+2\tilde{a}$	$\frac{2}{3}(3a+2\tilde{a})$	$\frac{1}{9}(3a+2\tilde{a})$
$B^{*0}\to B^0\gamma$	$-2(3a+\tilde{a})$	$-\frac{4}{3}(3a-\tilde{a})$	$-\frac{2}{9}(3a-\tilde{a})$	$3a-\tilde{a}$	$\frac{2}{3}(3a-\tilde{a})$	$\frac{1}{9}(3a-\tilde{a})$
$B^{*0}_s\to B^0_s\gamma$	0	$-\frac{4}{3}(6a+\tilde{a})$	$-\frac{8}{9}(3a-\tilde{a})$	0	$\frac{4}{3}(3a-\tilde{a})$	$\frac{4}{9}(3a-\tilde{a})$

TABLE XIV. The flavor-dependent coefficients $\mathcal{C}_\phi^{(x)}(x=a,c,d,e)$ in Eqs. (68)–(72) for the B^* mesons.

States	$\mathcal{C}_\pi^{(a)}$	$\mathcal{C}_K^{(a)}$	$\mathcal{C}_\pi^{(c)}$	$\mathcal{C}_K^{(c)}$	$\mathcal{C}_\pi^{(d)}$	$\mathcal{C}_K^{(d)}$	$\mathcal{C}_\pi^{(e)}$	$\mathcal{C}_K^{(e)}$	$\mathcal{C}_\eta^{(e)}$
B^{*+}	$-\frac{1}{2}$	$-\frac{1}{2}$	2	2	−2	−2	$-3a$	$-\frac{2}{3}(3a-\tilde{a})$	$-\frac{1}{9}(3a+2\tilde{a})$
B^{*0}	$\frac{1}{2}$	0	−2	0	2	0	$-(3a+\tilde{a})$	$-\frac{2}{3}(3a-\tilde{a})$	$-\frac{1}{9}(3a-\tilde{a})$
B_s^{*0}	0	$\frac{1}{2}$	0	−2	0	2	0	$-\frac{2}{3}(6a+\tilde{a})$	$-\frac{4}{9}(3a-\tilde{a})$

TABLE XV. The flavor-dependent coefficients $\mathcal{C}_\phi^{(x)}(x=g,l+m)$ in Eqs. (74)–(76) for the B^* mesons.

States	$\mathcal{C}_\pi^{(g)}$	$\mathcal{C}_K^{(g)}$	$\mathcal{C}_\eta^{(g)}$	$\mathcal{C}_\pi^{(lm)}$	$\mathcal{C}_K^{(lm)}$	$\mathcal{C}_\eta^{(lm)}$
B^{*+}	$-3a$	$-\frac{2}{3}(3a+\tilde{a})$	$-\frac{1}{9}(3a-2\tilde{a})$	$\frac{1}{2}(2\tilde{a}-3a)$	$\frac{1}{3}(2\tilde{a}-3a)$	$\frac{1}{18}(2\tilde{a}-3a)$
B^{*0}	$-(3a-\tilde{a})$	$-\frac{2}{3}(3a+\tilde{a})$	$-\frac{1}{9}(3a+\tilde{a})$	$-\frac{1}{2}(3a+\tilde{a})$	$-\frac{1}{3}(3a+\tilde{a})$	$-\frac{1}{18}(3a+\tilde{a})$
B_s^{*0}	0	$-\frac{2}{3}(6a-\tilde{a})$	$-\frac{4}{9}(3a+\tilde{a})$	0	$-\frac{2}{3}(3a+\tilde{a})$	$-\frac{2}{9}(3a+\tilde{a})$

APPENDIX B: LOOP INTEGRALS

Here, we show the detailed forms of the $\mathcal{J}$ functions used in the text. One can find the complete forms in Ref. [58].

$$i\int\frac{d^Dl\lambda^{4-D}}{(2\pi)^D}\frac{1}{l^2-m^2+i\varepsilon}\equiv\mathcal{J}_0^c(m), \tag{B1}$$

$$i\int\frac{d^Dl\lambda^{4-D}}{(2\pi)^D}\frac{l^\alpha l^\beta}{(v\cdot l+\omega+i\varepsilon)(l^2-m^2+i\varepsilon)} \equiv[v^\alpha v^\beta\mathcal{J}_{21}^a+g^{\alpha\beta}\mathcal{J}_{22}^a](m,\omega), \tag{B2}$$

$$i\int\frac{d^Dl\lambda^{4-D}}{(2\pi)^D}\frac{l^\alpha l^\beta}{(v\cdot l+\omega+i\varepsilon)[v\cdot l+\delta+i\varepsilon](l^2-m^2+i\varepsilon)} \equiv[v^\alpha v^\beta\mathcal{J}_{21}^g+g^{\alpha\beta}\mathcal{J}_{22}^g](m,\omega,\delta), \tag{B3}$$

$$i\int\frac{d^Dl\lambda^{4-D}}{(2\pi)^D}\frac{l^\alpha l^\beta}{(l^2-m^2+i\varepsilon)[(l+q)^2-m^2+i\varepsilon]} \equiv[q^\alpha q^\beta\mathcal{J}_{21}^F+g^{\alpha\beta}\mathcal{J}_{22}^F](m,q), \tag{B4}$$

$$i\int\frac{d^Dl\lambda^{4-D}}{(2\pi)^D}\frac{l^\alpha l^\beta}{(v\cdot l+\omega+i\varepsilon)(l^2-m^2+i\varepsilon)[(l+q)^2-m^2+i\varepsilon]} \equiv[g^{\alpha\beta}\mathcal{J}_{21}^T+q^\alpha q^\beta\mathcal{J}_{22}^T+v^\alpha v^\beta\mathcal{J}_{23}^T+(q\vee v)\mathcal{J}_{24}^T](m,\omega,q), \tag{B5}$$

where $q\vee v\equiv q^\alpha v^\beta+q^\beta v^\alpha$. The $\mathcal{J}$ functions defined above can be calculated with the dimensional regularization in D dimensions. In the following, we write out the expressions of the used $\mathcal{J}$ functions:

$$\mathcal{J}_0^c(m)=2m^2L+\frac{m^2}{16\pi^2}\ln\frac{m^2}{\lambda^2}, \tag{B6}$$

$$\mathcal{J}_{22}^a(m,\omega)=2\omega\left(m^2-\frac{2}{3}\omega^2\right)L+\frac{1}{16\pi^2}\int_{-\omega}^0\tilde{\Delta}\ln\frac{\tilde{\Delta}}{\lambda^2}dy+\frac{1}{24\pi}\tilde{A}^{3/2}, \tag{B7}$$

$$\mathcal{J}_{22}^g(m,\omega,\delta)=\begin{cases}\frac{1}{\delta-\omega}[\mathcal{J}_{22}^a(m,\omega)-\mathcal{J}_{22}^a(m,\delta)] & \text{if } \omega\neq\delta\\ -\frac{\partial}{\partial x}\mathcal{J}_{22}^a(m,x)|_{x\to\omega(\text{ or }\delta)} & \text{if } \omega=\delta\end{cases}, \tag{B8}$$

$$\mathcal{J}_{22}^F(m,q)=\left(m^2-\frac{q^2}{6}\right)L+\frac{1}{32\pi^2}\int_0^1\bar{\Delta}\ln\frac{\bar{\Delta}}{\lambda^2}dx, \tag{B9}$$

$$\mathcal{J}_{21}^T(m,\omega,q)=2\omega L+\frac{1}{16\pi^2}\int_0^1dx\int_{-\omega}^0\left(1+\ln\frac{\Delta}{\lambda^2}\right)dy+\frac{1}{16\pi}\int_0^1A^{1/2}dx, \tag{B10}$$

where $\tilde{\Delta}=y^2+\tilde{A}$, $\tilde{A}=m^2-\omega^2-i\varepsilon$; $\bar{\Delta}=x(x-1)q^2+m^2-i\varepsilon$; $\Delta=y^2+A$, $A=x(x-1)q^2+m^2-(\omega-xq_0)^2-i\varepsilon$.

L is defined as

$$L=\frac{1}{16\pi^2}\left[\frac{1}{D-4}+\frac{1}{2}(\gamma_E-1-\ln4\pi)\right], \tag{B11}$$

where γ_E is the Euler-Mascheroni constant 0.5772157. We adopt the modified minimal subtraction ($\overline{\text{MS}}$) scheme to renormalize the loop integrals, which is equivalent to making use of the following relation:

$$\{X\}_r = \lim_{D\to 4}\left(X - L\frac{\partial}{\partial L}X\right) + \frac{1}{16\pi^2}\lim_{D\to 4}\left(\frac{\partial}{\partial D}\frac{\partial}{\partial L}X\right), \tag{B12}$$

where $\{X\}_r$ represents the finite part of X.

APPENDIX C: ESTIMATING THE LIGHT QUARK MASS WITH THE VECTOR MESON DOMINANCE MODEL

In general, the transition form factor of $V \to P\gamma$ at the leading order can be parameterized as follows:

$$\mu'_{\bar{Q}q} = \mathcal{Q}_{\bar{Q}}\frac{1}{\Lambda_{\bar{Q}}} - \mathcal{Q}_q\frac{1}{\Lambda_q}, \tag{C1}$$

where $\mathcal{Q}_{\bar{Q}}$ and $\mathcal{Q}_q$ denote the charge matrices of $\bar{Q}$ and q, respectively. $\Lambda_{\bar{Q}}$ and Λ_q are the mass parameters that can be understood as the masses of the constituent quarks in the quark model. Heavy quark symmetry guarantees $\Lambda_{\bar{Q}} \approx m_{\bar{Q}}$ (see the discussions in Ref. [51]). However, the photon coupling to the light quark part of the electromagnetic current is not fixed by the heavy quark symmetry; thus, the Λ_q is not a "well defined" constant—its value is largely model dependent to some extent. Here, we adopt the vector meson dominance (VMD) model [3,16] to estimate the value of Λ_q.

In the VMD model, the light quark part of the electromagnetic current $\langle P|J^\ell_\mu|V\rangle$ can be expressed as follows by inserting the light vector resonance $\mathcal{V}$:

$$\begin{aligned}&\langle P_a(p')|J^\ell_\mu(q^2)|V_a(p,\varepsilon_V)\rangle \\ &= ie_a\sum_{\mathcal{V},\lambda}\frac{\langle 0|\bar{q}_a\gamma_\mu q_a|\mathcal{V}(q,\varepsilon^\lambda_\mathcal{V})\rangle}{q^2 - m^2_\mathcal{V}}\langle P_a(p')\mathcal{V}(q,\varepsilon^\lambda_\mathcal{V})|V_a(p,\varepsilon_V)\rangle,\end{aligned} \tag{C2}$$

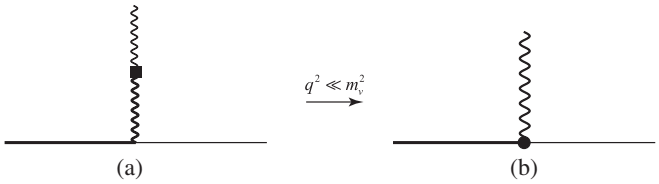

FIG. 6. A diagrammatic presentation of the vector meson dominance model. The thick wiggly line in diagram (a) denotes the light vector meson ρ or ϕ, while the solid square denotes the coupling vertex of the photon and light vector meson. Other notations are the same as those in Fig. 2.

where the $\langle P_a\mathcal{V}|V_a\rangle$ vertex is given in Eq. (54). [A diagrammatic presentation of Eq. (C2) is shown in Fig. 6.] The matrix element $\langle 0|\bar{q}_a\gamma_\mu q_a|\mathcal{V}(q,\varepsilon^\lambda_\mathcal{V})\rangle$ can be calculated by assuming the SU(3) symmetry with

$$\langle 0|\bar{q}_a\gamma_\mu q_a|\mathcal{V}(q,\varepsilon^\lambda_\mathcal{V})\rangle = f_\mathcal{V}\varepsilon^\mu_\mathcal{V}\mathrm{Tr}(\mathcal{V}T^a), \tag{C3}$$

where $f_\mathcal{V}$ and $\varepsilon_\mathcal{V}$ denote the decay constant and polarization vector of the light vector meson, respectively. $(T^a)_{lm} = \delta_{al}\delta_{am}$, and $a = 1, 2, 3$ for u, d, s, respectively. The $f_\mathcal{V}$ can be determined by the electromagnetic decay $\mathcal{V} \to e^+e^-$. $f_\rho = 0.17\ \mathrm{GeV}^2$ for the ρ meson, and $f_\phi = 0.25\ \mathrm{GeV}^2$ for the ϕ meson [16].

Following the same procedure in obtaining Eq. (53), one can get

$$\Lambda_q^{-1} = 2\sqrt{2}g_v\lambda\sqrt{\frac{m_V}{m_P}}\frac{f_\mathcal{V}}{m^2_\mathcal{V}}, \tag{C4}$$

where the values of g_v and λ are the same as those in Eq. (58). One can obtain Λ_q by considering the SU(3)-breaking effect in Eq. (C4), eventually:

$$\Lambda_u = \Lambda_d = 0.366\ \mathrm{GeV}, \qquad \Lambda_s = 0.596\ \mathrm{GeV}. \tag{C5}$$

These values are very close to the m_u, m_d, and m_s given in Eq. (59).

[1] H. Y. Gao, Nucleon electromagnetic form-factors, Int. J. Mod. Phys. E **12**, 1 (2003).
[2] J. Arrington, C. D. Roberts, and J. M. Zanotti, Nucleon electromagnetic form-factors, J. Phys. G **34**, S23 (2007).
[3] S. Pacetti, R. B. Ferroli, and E. Tomasi-Gustafsson, Proton electromagnetic form factors: Basic notions, present achievements and future perspectives, Phys. Rep. **550–551**, 1 (2015).
[4] T. Chupp, P. Fierlinger, M. Ramsey-Musolf, and J. Singh, Electric dipole moments of atoms, molecules, nuclei, and particles, Rev. Mod. Phys. **91**, 015001 (2019).
[5] H. X. Chen, W. Chen, X. Liu, and S. L. Zhu, The hidden-charm pentaquark and tetraquark states, Phys. Rep. **639**, 1 (2016).
[6] F. K. Guo, C. Hanhart, U. G. Meissner, Q. Wang, Q. Zhao, and B. S. Zou, Hadronic molecules, Rev. Mod. Phys. **90**, 015004 (2018).
[7] Y. R. Liu, H. X. Chen, W. Chen, X. Liu, and S. L. Zhu, Pentaquark and tetraquark states, Prog. Part. Nucl. Phys. **107**, 237 (2019).
[8] M. E. Peskin and D. V. Schroeder, *An Introduction to Quantum Field Theory* (World Publishing Corporation, Beijing, 2007), p. 184.

[9] M. Tanabashi *et al.* (Particle Data Group), Review of particle physics, Phys. Rev. D **98**, 030001 (2018).

[10] E. Sucipto and R. L. Thews, Radiative decay systematics and flavor symmetry breaking from heavy quarks, Phys. Rev. D **36**, 2074 (1987).

[11] A. N. Kamal and Q. P. Xu, Total width of the D^*, Phys. Lett. B **284**, 421 (1992).

[12] M. A. Ivanov and Y. M. Valit, Radiative and hadronic decays of heavy vector mesons, Z. Phys. C **67**, 633 (1995).

[13] W. Jaus, Semileptonic, radiative, and pionic decays of B, B^* and D, D^* mesons, Phys. Rev. D **53**, 1349 (1996).

[14] H. M. Choi, Decay constants and radiative decays of heavy mesons in light-front quark model, Phys. Rev. D **75**, 073016 (2007).

[15] M. Priyadarsini, P. C. Dash, S. Kar, S. P. Patra, and N. Barik, Electromagnetic form factors of heavy flavored vector mesons, Phys. Rev. D **94**, 113011 (2016).

[16] P. Colangelo, F. De Fazio, and G. Nardulli, Radiative heavy meson transitions, Phys. Lett. B **316**, 555 (1993).

[17] S. Godfrey and N. Isgur, Mesons in a relativized quark model with chromodynamics, Phys. Rev. D **32**, 189 (1985).

[18] J. L. Goity and W. Roberts, Radiative transitions in heavy mesons in a relativistic quark model, Phys. Rev. D **64**, 094007 (2001).

[19] D. Ebert, R. N. Faustov, and V. O. Galkin, Radiative M1 decays of heavy light mesons in the relativistic quark model, Phys. Lett. B **537**, 241 (2002).

[20] S. K. Bose and L. P. Singh, Magnetic moments of charmed and b flavored hadrons in MIT bag model, Phys. Rev. D **22**, 773 (1980).

[21] V. Simonis, Magnetic properties of ground-state mesons, Eur. Phys. J. A **52**, 90 (2016).

[22] V. Simonis, Improved predictions for magnetic moments and M1 decay widths of heavy hadrons, arXiv:1803.01809.

[23] T. M. Aliev, E. Iltan, and N. K. Pak, Radiative D^* meson decays in QCD sum rules, Phys. Lett. B **334**, 169 (1994).

[24] H. G. Dosch and S. Narison, $B^*B\pi(\gamma)$ couplings and $D^* \to D\pi(\gamma)$ decays within a $1/M$ expansion in full QCD, Phys. Lett. B **368**, 163 (1996).

[25] S. L. Zhu, W. Y. P. Hwang, and Z. S. Yang, $D^* \to D\gamma$ and $B^* \to B\gamma$ as derived from QCD sum rules, Mod. Phys. Lett. A **12**, 3027 (1997).

[26] D. Becirevic and B. Haas, $D^* \to D\pi$ and $D^* \to D\gamma$ decays: Axial coupling and magnetic moment of D^* meson, Eur. Phys. J. C **71**, 1734 (2011).

[27] A. Deandrea, N. Di Bartolomeo, R. Gatto, G. Nardulli, and A. D. Polosa, A constituent quark meson model for heavy meson processes, Phys. Rev. D **58**, 034004 (1998).

[28] P. L. Cho and H. Georgi, Electromagnetic interactions in heavy hadron chiral theory, Phys. Lett. B **296**, 408 (1992).

[29] H. Y. Cheng, C. Y. Cheung, G. L. Lin, Y. C. Lin, T. M. Yan, and H. L. Yu, Chiral Lagrangians for radiative decays of heavy hadrons, Phys. Rev. D **47**, 1030 (1993).

[30] J. F. Amundson, C. G. Boyd, E. E. Jenkins, M. E. Luke, A. V. Manohar, J. L. Rosner, M. J. Savage, and M. B. Wise, Radiative D^* decay using heavy quark and chiral symmetry, Phys. Lett. B **296**, 415 (1992).

[31] R. Casalbuoni, A. Deandrea, N. Di Bartolomeo, R. Gatto, F. Feruglio, and G. Nardulli, Phenomenology of heavy meson chiral Lagrangians, Phys. Rep. **281**, 145 (1997).

[32] H. B. Deng, X. L. Chen, and W. Z. Deng, Meson decays in an extended Nambu–Jona-Lasinio model with heavy quark flavors, Chin. Phys. C **38**, 013103 (2014).

[33] Y. L. Luan, X. L. Chen, and W. Z. Deng, Meson electromagnetic form factors in an extended Nambu–Jona-Lasinio model including heavy quark flavors, Chin. Phys. C **39**, 113103 (2015).

[34] E. E. Jenkins, M. E. Luke, A. V. Manohar, and M. J. Savage, Chiral perturbation theory analysis of the baryon magnetic moments, Phys. Lett. B **302**, 482 (1993).

[35] U. G. Meissner and S. Steininger, Baryon magnetic moments in chiral perturbation theory, Nucl. Phys. **B499**, 349 (1997).

[36] H. S. Li, L. Meng, Z. W. Liu, and S. L. Zhu, Magnetic moments of the doubly charmed and bottom baryons, Phys. Rev. D **96**, 076011 (2017).

[37] H. S. Li, L. Meng, Z. W. Liu, and S. L. Zhu, Radiative decays of the doubly charmed baryons in chiral perturbation theory, Phys. Lett. B **777**, 169 (2018).

[38] L. Meng, H. S. Li, Z. W. Liu, and S. L. Zhu, Magnetic moments of the spin-$\frac{3}{2}$ doubly heavy baryons, Eur. Phys. J. C **77**, 869 (2017).

[39] A. N. H. Blin, Z. F. Sun, and M. J. V. Vacas, Electromagnetic form factors of spin-1/2 doubly charmed baryons, Phys. Rev. D **98**, 054025 (2018).

[40] N. Jiang, X. L. Chen, and S. L. Zhu, Electromagnetic decays of the charmed and bottom baryons in chiral perturbation theory, Phys. Rev. D **92**, 054017 (2015).

[41] G. J. Wang, L. Meng, H. S. Li, Z. W. Liu, and S. L. Zhu, Magnetic moments of the spin-$\frac{1}{2}$ singly charmed baryons in chiral perturbation theory, Phys. Rev. D **98**, 054026 (2018).

[42] L. Meng, G. J. Wang, C. Z. Leng, Z. W. Liu, and S. L. Zhu, Magnetic moments of the spin-$\frac{3}{2}$ singly heavy baryons, Phys. Rev. D **98**, 094013 (2018).

[43] G. J. Wang, L. Meng, and S. L. Zhu, Radiative decays of the singly heavy baryons in chiral perturbation theory, Phys. Rev. D **99**, 034021 (2019).

[44] G. S. Yang and H. C. Kim, Magnetic moments of the lowest-lying singly heavy baryons, Phys. Lett. B **781**, 601 (2018).

[45] J. Y. Kim and H. C. Kim, Electromagnetic form factors of singly heavy baryons in the self-consistent SU(3) chiral quark-soliton model, Phys. Rev. D **97**, 114009 (2018).

[46] R. G. Arnold, C. E. Carlson, and F. Gross, Elastic electron-deuteron scattering at high energy, Phys. Rev. C **21**, 1426 (1980).

[47] B. Wang, X. Liu, and D. Y. Chen, Prediction of anomalous $\Upsilon(5S) \to \Upsilon(1^3D_J)\eta$ transitions, Phys. Rev. D **94**, 094039 (2016).

[48] D. Coffman *et al.* (MARK-III Collaboration), Measurements of J/ψ decays into a vector and a pseudoscalar meson, Phys. Rev. D **38**, 2695 (1988); Erratum, Phys. Rev. D **40**, 3788(E) (1989).

[49] J. Jousset *et al.* (DM2 Collaboration), The $J/\psi \to$ vector + pseudoscalar decays and the η, η' quark content, Phys. Rev. D **41**, 1389 (1990).

[50] M. B. Wise, Chiral perturbation theory for hadrons containing a heavy quark, Phys. Rev. D **45**, R2188 (1992).

[51] A. V. Manohar and M. B. Wise, Heavy quark physics, Cambridge Monogr. Part. Phys., Nucl. Phys., Cosmol. **10**, 1 (2000).

[52] S. Ahmed *et al.* (CLEO Collaboration), First measurement of $\Gamma(D^{*+})$, Phys. Rev. Lett. **87**, 251801 (2001).
[53] H. Ohki, H. Matsufuru, and T. Onogi, Determination of $B^*B\pi$ coupling in unquenched QCD, Phys. Rev. D **77**, 094509 (2008).
[54] W. Detmold, C. J. D. Lin, and S. Meinel, Calculation of the heavy-hadron axial couplings g_1, g_2 and g_3 using lattice QCD, Phys. Rev. D **85**, 114508 (2012).
[55] E. Epelbaum, U. G. Meissner, W. Gloeckle, and C. Elster, Resonance saturation for four nucleon operators, Phys. Rev. C **65**, 044001 (2002).
[56] G. Ecker, J. Gasser, A. Pich, and E. de Rafael, The role of resonances in chiral perturbation theory, Nucl. Phys. **B321**, 311 (1989).
[57] N. Li, Z. F. Sun, X. Liu, and S. L. Zhu, Coupled-channel analysis of the possible $D^{(*)}D^{(*)}$, $\bar{B}^{(*)}\bar{B}^{(*)}$ and $D^{(*)}\bar{B}^{(*)}$ molecular states, Phys. Rev. D **88**, 114008 (2013).
[58] B. Wang, Z. W. Liu, and X. Liu, $\bar{B}^{(*)}\bar{B}^{(*)}$ interactions in chiral effective field theory, Phys. Rev. D **99**, 036007 (2019).
[59] E. Eichten, K. Gottfried, T. Kinoshita, K. D. Lane, and T. M. Yan, Charmonium: Comparison with experiment, Phys. Rev. D **21**, 203 (1980).